A Parametric Design of Ball End Mill

and Simulating Process

Liyong Chang

A Thesis

In the Department

of

Mechanical and Industrial Engineering

Presented in Partial Fulfillment of the Requirements

For the Degree of Master of Applied Science at

Concordia University

Montreal, Quebec, Canada

March 2016

CONCORDIA UNIVERSITY

School of Graduate Studies

This is to certify that the thesis prepared

By: Liyong Chang

Entitled: A Parametric Design of Ball end mill and Simulating Process

and submitted in partial fulfillment of the requirements for the degree of

Master of Applied Science

complies with the regulations of the University and meets the accepted standards with

respect to originality and quality.

Signed by the final examining committee:

_____Dr. Onur Kuzgunkaya_____Chair

_____Dr. Liangzhu Wang_____ Examiner

_____Dr. Wenfang Xie_____Examiner

_____Dr. Z. C. Chen_____ Supervisor

Approved by

_____

Chair of Department or Graduate Program Director

_____

Dean of Faculty

Date   _____

ABSTRACT

A Parametric Design of Ball End Mill and Simulating Process

Liyong Chang

Ball end mill cutter is widely used in precise CNC machining as a high efficiency processing tool for complex surface. On the basis of the literature review about mathematical model, grinding machining process, cutting experiment of ball end mills, and the calculation for a ball end mill, a ball end mill parametric design system is built by development technology with CATIA 3D modeling software and Visual Basic. With this system obtaining the model of the ball end mill, the simulation is processed in Third Wave AdvantEdge software.

The main contents of this paper are:

1. On the basis of creating a mathematical model of a ball end mill cutting edge curve, we generate the 3D model of the cutter in CATIA. Moreover, the conditions of the engagement between the grinding wheel and rake surface to avoid interference are proposed. As a result, the grinding wheel center location and orientation axis are defined.

2. A modeling program for ball end mills is developed in Visual Basic, and the

parameter modification can be visualized in the interface of this program .In addition, the model is simulated in Third Wave AdvantEdge to analyze the temperature of the cutter and the cutting force distribution.

KEY WORDS: Ball End Mill, Parametric Design, CATIA Secondary Development, Simulation

ACKNOWLEDGEMENTS

I hereby would like to thank my supervisor, Dr. Chevy Chen, for his kind guidance and patient instructions through all this work. It really improves me quite a lot going through all this research, I would not accomplish thesis without him.

Additionally, I would like to express my appreciation to all my dear colleagues in our lab, for every generous help from everyone when I encountered any problems.

Finally, I give my special thanks to my parents, for all their selfless love and continuous support in every aspect all through my study.

Table of Contents

List of Figures

List of Tables

Chapter 1. Introduction

1.1   Ball End-mill Background

End mill cutter, is playing a vital role in machining process in industry world. Due to the high paces of manufacturing development, the continuously growing varieties of material and the complexity of component geometry, end milling tools need to step into a higher level of conditions. In recent years, various end milling tools are adopted in industry, such as flat mill, ball end mill, fillet mill as shown in Figure 1.1. Even if some

Flat Nose   Ball Nose   Bull Nose   Chamfer
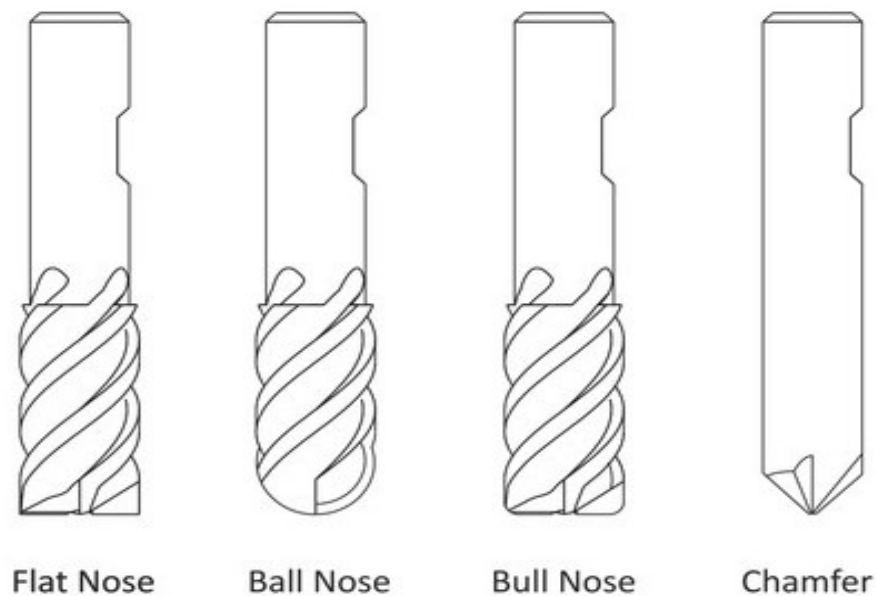
Figure 1.1 End Mill Tools Types

new manufacturing tools or even manufacturing methods spring up, end milling tools still have irreplaceable advantages.

Ball end mill used in a Computer Numerical Control (CNC) machine has been widely applied in High-Speed Machining (HSM) process. Additionally, ball end mill is an important kind of tool in machining complex three-dimensional surface. Due to its unique cutting edge shape (S-type, Helix-type, etc), ball end mill has the advantages of high machining precision, long product life, low manufacturing process cost, and it is able to axially feed. In a word, it meets the requirements for automatic processing of complex spatial surfaces.

Figure1.2 Ball End Mill Machining On a Work Piece

As shown in Fig 1.2, a ball end mill can be used in manufacturing a sphere in a work

piece, and the surface is much better than the one manufactured by other kinds of mill tools. This is just a sample, ball end mill can be widely applied in milling various shapes.

Definitely, all the expected advantages will be realized when the tools are well designed. Designing ball end mills has its unique obstacles, which will be discussed in next chapters. A model of ball end mill displayed in a 3D modeling software is shown in Fig 1.3.

Figure1.3 3D Ball End Mill Model in CATIA

1.2 Mathematical Model

The performance of a ball end mill in machining process is determined by the shapes of rake face and clearance face. Based on the mathematical model of the cutting edge of the ball end mill, rake face and clearance face can be defined by rake angle and

clearance angle respectively in the orthogonal sections. Afterwards, the grinding wheel locations can be determined by this mathematical model. It is necessary to create the mathematical model of the cutting edge and inspect it visually in Matlab. Based on the right mathematical model, it is time-saving to proceed the design.

In design process, mathematical calculation is the basis. Compared with feature-based design, because the cutting edge mathematical model is created at the very beginning in this method, it is more productive to calculate the data of manufacturing process. The basic connection of CAD and CAM can be built in this way, and that will be discussed in Chapter 3.

1.3   Parametric design

In general, a mechanical part consists of a couple of geometric features related to its function and its manufacturing method. Now, a kernel technique of the computer-aided design is parametric part design and modeling. On the basis of a new trend of mechanical part design-the part feature optimization, feature-based parametric part design is a dispensable advanced technique since the parametric CAD models of the part features can be easily modified in the part design optimization process. Therefore, the parametric part modeling function in the commercial CAD/CAM software is very important. By definition, the parametric part design is to determine the critical feature dimensions as the parameters and to specify the relations among the parameters and other part dimensions. In the parametric modeling function of the CAD/CAM software,

the functions of defining parameters and constraints are developed, and the parametric part models can be constructed. By assigning data to the feature parameters, all dimensions are calculated, and the solid model of the part can be changed and updated in seconds.

Mechanical part design includes several decision-making processes and activities, which are involved in determining the shape and dimensions of a mechanical part. Generally, the development of a mechanical part has five sections: formulation, concept design, configuration design, parametric design, and detail design. With a parametric design of a part, the solid model of a part design can be easily attained, and the part can be analyzed to predict the part performance and functionality. This can significantly reduce the leading time in the part design cycle and the cost of making prototype. To implement the parametric part design and modeling, the following four procedures are necessary, which are

1) Defining the key dimensions as the parameters,

2) Fixing the relationships or constraints between the parameters and the part dimensions,

3) Building the part model in CAD/CAM software,

4) Inputting different parameters and the constraints to inspect the models.

1.4 Literature Review

There are a number of academic thesis that have proposed the modeling process of

the ball end mill. Kim and Park [1] have described a design process of an end mill. In their thesis, the solid model of a specific end mill is constructed together with the computation of the cutter's geometry, grinding wheel geometry, wheel positioning fabricating end mills withe the required cutter geometry. Tandon and Khan [2] present a three dimensional modeling and finite element simulation of a generic end mill. Their paper describes in detail the methodology to model the geometry of a end mill in terms of three-dimensional parameters. The geometric definition of the end mill is developed in terms of surface patches; flutes as helicoidal surfaces, the shank as a surface of revolution and the blending surfaces as bicubic Bezier and biparametric sweep surfaces. Lazoglu[3] developed a mechanical model of a ball end mill in the year of 2003, the model has the ability to calculate the workpiece/cutter intersection domain automatically for a given cutter location (CL) file, cutter and workpiece geometries, that helps to obtain experiences about the cutter working conditions. Altintas and Lee [4] have presented the mechanics and dynamics of cutter with helical ball end mills. The helical ball end mill attached to the spindle is modeled by orthogonal structural modes in the feed and normal directions at the tool tip. Vickers and Quan[5] showed how to give a better match to the required surface geometry and hence reduce the number of surface passes required. Zhu and Kapoor [6] gave a mechanical modeling of ball end mill process, in addition, they present an idea of multi-axis machining of free style surface. With regard to the simulation of the end mills, several papers are reviewed. Imani, Sadeghi and Elbestawi [7] developed a system that deals with the geometry and mechanics of machining with ball-end milling cutters. Moreover, this system can

generate the model of workpiece/cutter engagement. In Yucesan and Altintas[8] thesis, Mechanics of milling with ball ended helical cutters are modeled, which is based on the analytic representation of ball shaped helical flute geometry, and its rake and clearance surfaces. After that, their work focused on the prediction of the cutting forces. In Miyaguchi, Masuda, Takeoka and Iwabe [9] thesis, the research focused on the effect of stiffness upon tool wear in high spindle speed milling, and it is applied in small size of ball end mill. The specific force coefficients for a general end mill was discussed in Gradiš ek, Kalveram, and Weinert[10] thesis. Milfelner, Kopac, Cus and Zuperl [11] did a reseach about a genetic equation for the cutting force in ball-end milling in the year of 2005. Jin, Goto, Watanabe, Kurosawa,and Murakawa[12], developed a new cutting edge of CBN ball-nosed end mill. In Sharman, Dewes, and Aspinwall [13] thesis, tool life has been discussed when high speed is applied on ball nose end milling. Kangnin [14] built a rigid Cutting Force Model of Ball End Mill in the year of 1998, which help us to analyze the cutting force. In Jinling [15]'s study, the CNC Grinding of the Ball Nose End Mill, the grinding conditions have been introduced. Pa, Sarhan, and Shukor [16] showed a method of optimizing the cutting parameters for better surface of ball end mill. In references [17], [18], [19] and [20], the simulation for cutting force and temperature distribution on the end mill surface was studied. In Lazoglu and Liang's [21] thesis, the modeling of ball-end milling forces was applied with cutter axis inclination, the result of their experiment helped to reconsider the ball end mill shape. Aoyama, Kishinami, and Saito [22] developed a kind of ball end mill named elliptic ball end mill. Wang's [23] thesis, A new CAD/CAM/CAE integration approach to modeling flutes of solid end-mills,

helped us to calculate the flute profile points, which is the foundation of the flute modeling in cylinder part.

1.5 Objective of Thesis

As the configuration of the rake face and clearance face is quite decisive for a ball end mill, most works in this thesis will be focused on them. Accordingly, we build a mathematical model of the cutting edge curve, and program it in Matlab. In Matlab, this model can be analyzed and verified visually. From the design of the rake face and clearance face, the flute surface can be generated by a fixed grinding wheel. Additionally, it is a new method to determine the rake face by rake angle and the width of rake face in each cross sections, clearance face can be defined in same way.

It is time wasting to build different models in 3D modeling software when we need to modify a given model or compare the performance of two models. A ball end mill modeling software is proposed in this thesis. Different models can be generated automatically in this software by changing the values of the parameters.

On the basis of mathematical model of the cutting edge, the flute surface can be generated by a grinding wheel in the light of a tangency condition. Once we obtain the location coordinates of the wheel, Boolean operations can be applied in the 3D modeling software. Our goal is to get a method to make the surface continuous and precise.

In the end, a finite-element analysis simulation is applied to compare the different

models based on different parameters.

1.6   Thesis Outline

This thesis consists of several chapters. Chapter 1 introduces the basic knowledge of end mill tools, mathematical model of the cutting edge, parametric design, and the literature reviews about this thesis topic. Chapter 2 represents the mathematical model, the generation of the rake face and clearance face. Then discussion about the rake face parameters optimization is presented. Chapter 3 introduces the calculation of the location coordinates of the grinding wheel, followed by the modeling by Boolean operations. Then the method of optimizing flute surface is introduced. Chapter 4 shows simulation in a FEA software compared with two different models. Chapter 5 concludes the research and introduces the future work about this modeling method.

Chapter 2. Mathematical Model of Cutting Edge Curve

2.1 Parametric Equation

The accuracy of the products manufactured by a ball end mill relies on the precision of the cutting edge. Therefore, the cutting edge need to be designed and machined accurately. The goal of this section is to build the equations of the helix cutting edge curve of a ball end mill.

The cutting edge curve goes from the top of the sphere through the ball part and cylindrical part. A tool coordinate system OXYZ is built in a bar, in which the origin O is placed at sphere center, and the OZ axis coincides with the longitudinal axis of the bar. All of the following calculations are based on this coordinate system.

The cutting edge curve is shown in Fig 2.1. M_i is a general point along the cutting edge curve, and its coordinate can be presented as a vector OM_i as follows:

$$OM_i = \left[cos\varphi \cdot \sqrt{R^2 - z^2}, sin\varphi \cdot \sqrt{R^2 - z^2}, z \right]$$

Eq.(2-1)

In which R is the radius of the ball and φ is the virtual angle between the tool tip and the current M_i on the cutting edge curve.

Helix angle is the angle between the tangent vector of the longitudinal axis $\hat{T}_i$, and

the tangent vector of the helix T_i. The angle β represents the helix angle in this model. A

mathematical model of the cutting edge with a constant helix or a constant pitch was

developed previously. In our research, the constant helix is applied to the cutting edge

curve. Thus, the relation of the virtual angle φ and helix angle β can be described as

follows:

$$d\varphi = -\frac{tan\beta}{R}dz \qquad \text{Eq.(2-2)}$$

The virtual angle is zero at tool tip where $z = R$, and it can be obtained by calculation

the integral of Eq.(2-2):

$$\varphi = -\frac{tan\beta}{R}(z - R) \qquad \text{Eq.(2-3)}$$

Substituting the φ in Eq.(2-3) into Eq.(2-1), we can get the parameter equation of the

cutting edge curve:

$$\begin{cases} x(\varphi) = R \cdot cos\varphi \cdot \sqrt{1 - \left(1 - \dfrac{\varphi}{tan\beta}\right)^2} \\ y(\varphi) = R \cdot sin\varphi \cdot \sqrt{1 - \left(1 - \dfrac{\varphi}{tan\beta}\right)^2} \\ z(\varphi) = R \cdot \left(1 - \dfrac{\varphi}{tan\beta}\right) \end{cases} \qquad \text{Eq. (2-4)}$$

2.2 Application in Matlab

In this section, the manipulation of the parameter equation of the cutting edge

curve is described. Additionally, this process contributes to obtaining the precise cutting edge curve, and make it convenient in programming in Matlab to get the visualized analysis. Firstly, the equation can be added with several conditions on the basis of foundations of mathematics. The conditions will be presented as follows:

1) $\beta \neq 0$

2) $0 \leq \dfrac{\varphi}{\tan\beta} \leq 1$

Applying Eq.(2-4) and the conditions above in Matlab, the 3D configuration of the cutting edge can be described in Figure 2.1. In this graph, there are four cutting edges determined by four different helix angles shown on the sphere surface. From left to right, four curves in white, yellow, green and black represent the cases in terms of variable helix angle, and the value is $\beta_{white} = 28.65°$, $\beta_{yellow} = 40.11°$, $\beta_{green} = 51.57°$, $\beta_{black} = 63.03°$, respectively.
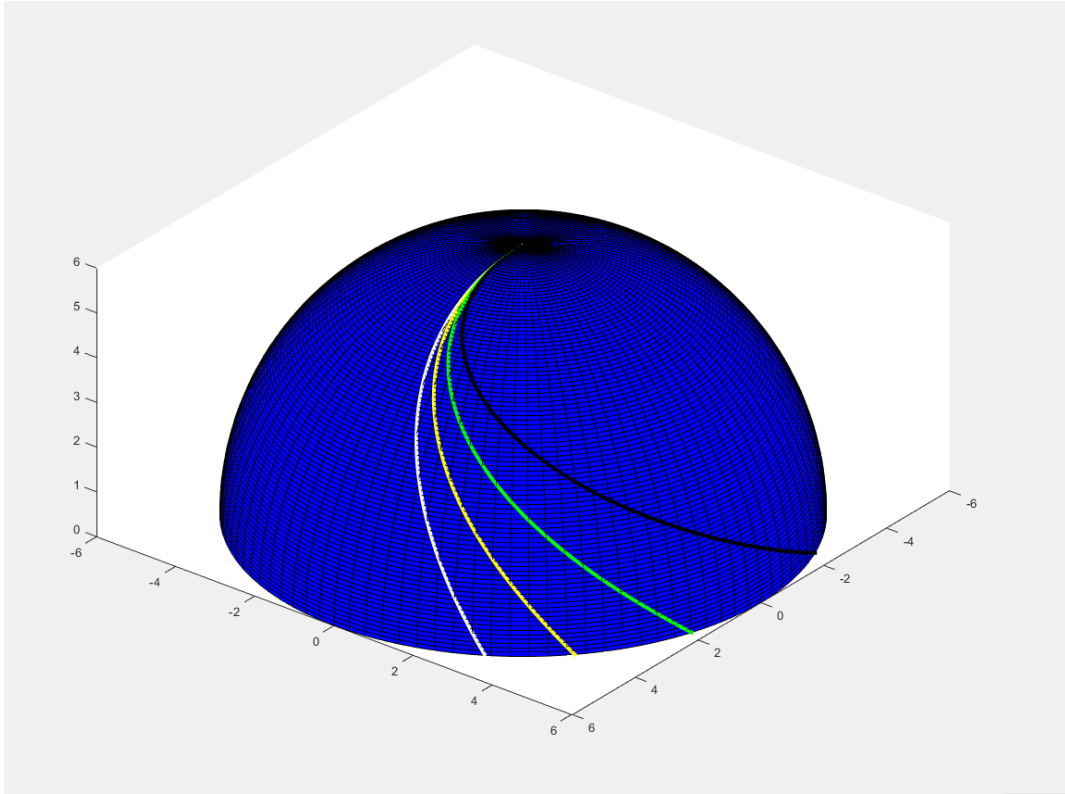
Figure 2.1 Cutting Edge Curve Visualized in Matlab

In Figure 2.2, the curvature in disperse helix angle determining situations can be clearly detected. With the helix angle increasing, apparently, the performance of a ball end mill will be influenced. The specific influences will be discussed in the simulation chapter, Chapter 5.
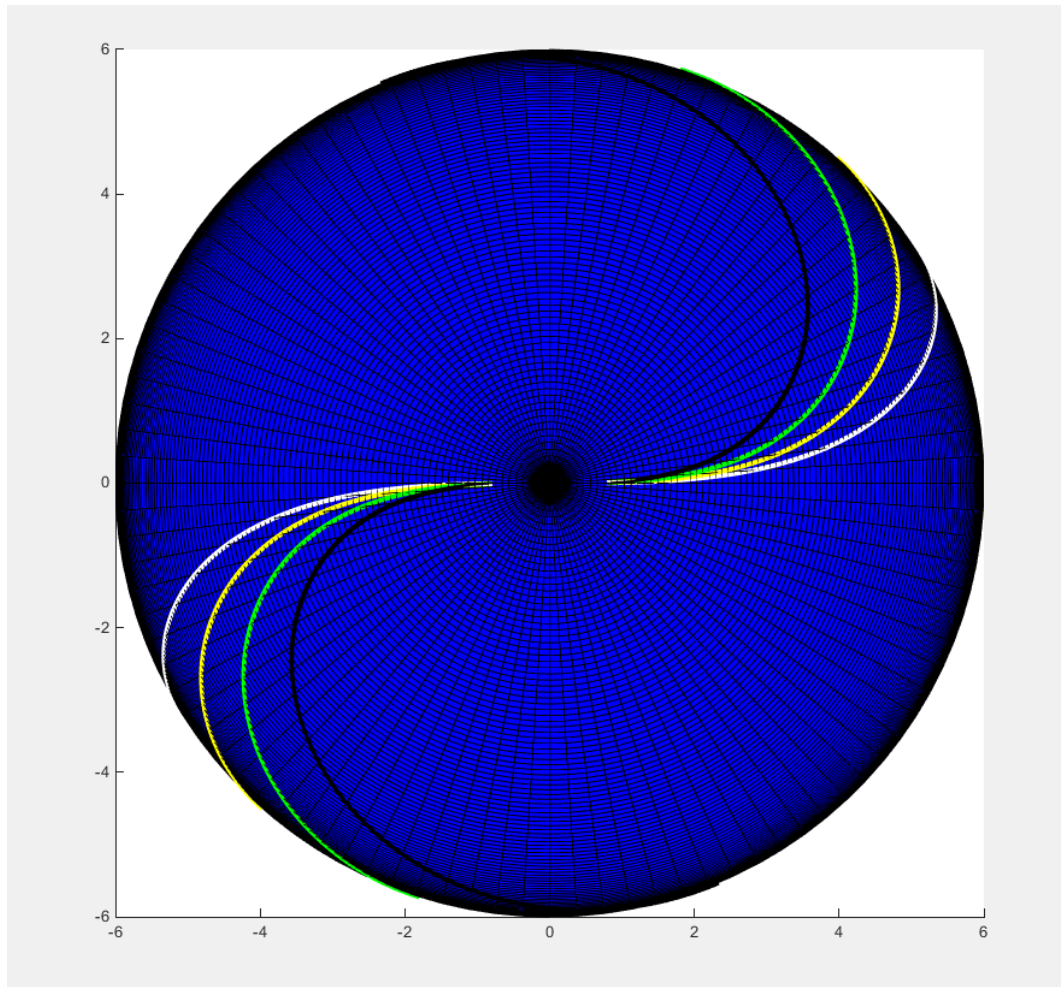
Figure 2.2 Cutting Edge Curve Visualized in Matlab (Top View)

Chapter 3. Mathematical Model of Ball End Mill

3.1 Introduction

In this chapter, the basic components of the ball part will be modeled mathematically. It is divided in rake face design and clearance face design. In each part,
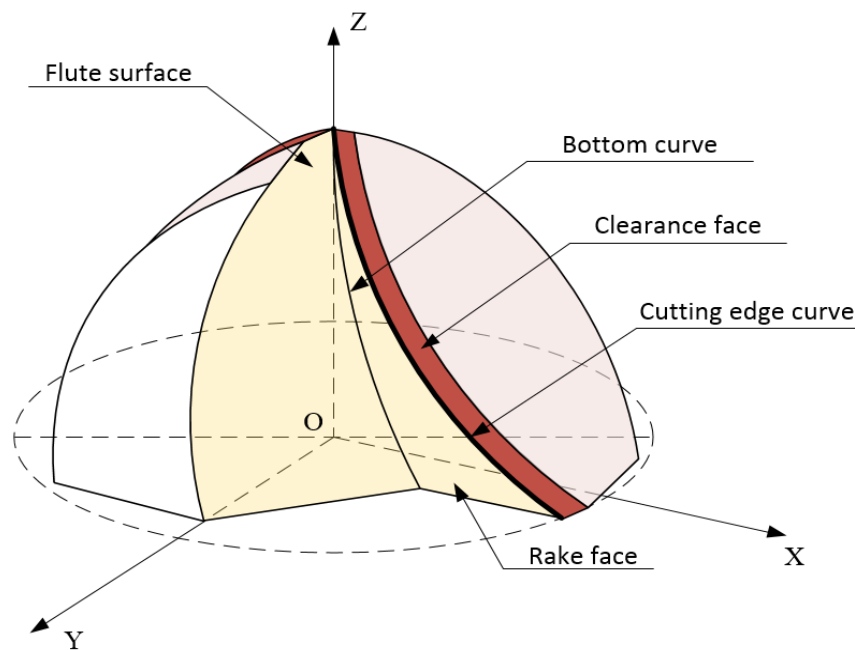
Figure 3.1 Basic Components of Ball Part

The equations will be determined first, and then verified in CATIA by coding in VB.NET. The ball part components are shown in Fig 3.1.

Wheel locations for the rake face part and clearance part are definitely important for machining. Thus, they will be calculated and analyzed in this chapter.

3.2 Toolbar Modeling and the Construction of Coordinate System

Our purpose is to precisely machine a ball end mill, and the basic parameters of the product, i.e. radius of the ball part, length of cutter, are determined by the toolbar parameters settings.

In this paper, the radius of the bar R, and the length of the bar L are set as follows:

$R = 6mm, \ L = 80mm$

The calculations of the ball end mill components, i.e. cutting edge, rake face, clearance face, are on the basis of coordinate system OXYZ. The center of the hemisphere of the ball part is defined as the origin of this coordinate system OXYZ, and the axis of the toolbar is determined as the Z-axis. They can be described in Fig 3.2.
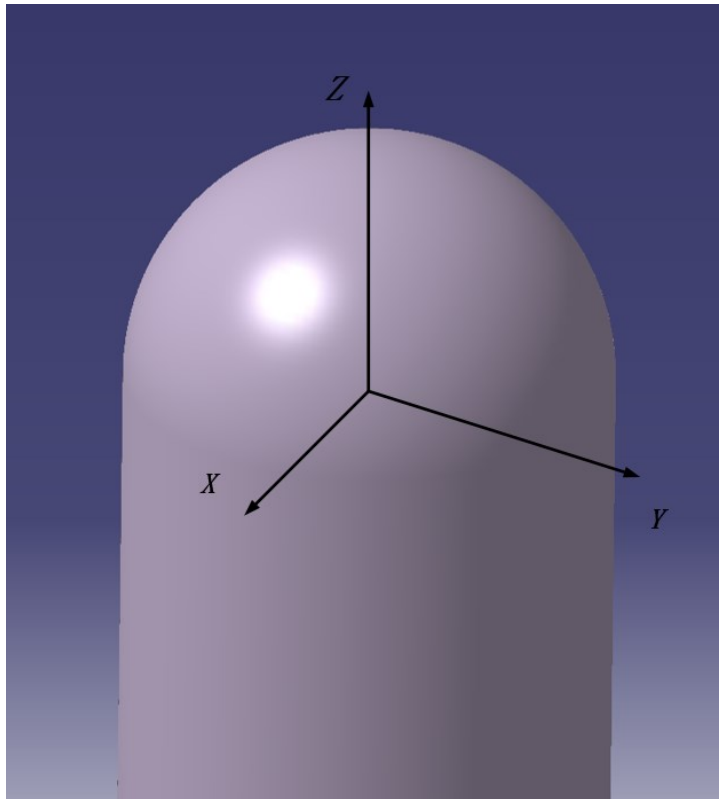
Figure 3.2 Toolbar Location in Coordinate System

The radius and length can be edited in designed Visual Basic interface, and that will be introduced in next chapter.

3.3 Mathematical Model of Rake Face in Ball Part

In this section, the tangent and normal vectors to the spherical surface along the cutting edge are introduced as the basic components of the cutting edge curve. As shown in Fig 3.3.
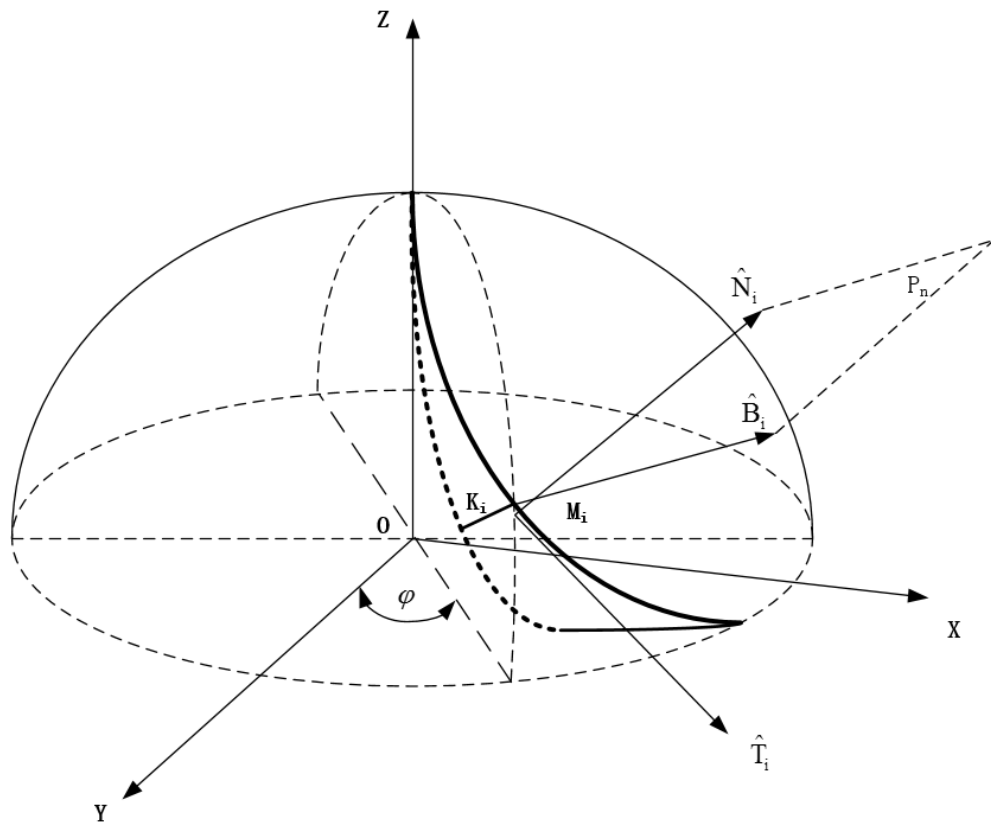
Figure 3.3 Geometric Component on Cutting Edge

On the basis of designed depth of cut in the normal plane of cutting edge, a bottom

curve is defined, which is important for determining the wheel locations for the rake

face, and it will be introduced in Section 3.3.

The tangent vector of the Cutting edge $\hat{T}_i$, the normal vector of the ball surface $\hat{N}_i$,

and the vector $\hat{C}_i$, which is the cross product of the vector $\hat{T}_i$ and vector $\hat{N}_i$. Point M_i is

defined as a general point of the cutting edge. On the basis of the position vector

$m = [x, y, z]$ of a general point along the cutting edge, the vectors $\hat{T}_i$, $\hat{N}_i$ and $\hat{C}_i$ can be

described by Eq(3-1):

$$\begin{cases} \hat{T}_i = \dfrac{\dot{m}}{|\dot{m}|} = \begin{bmatrix} T_{xi}, T_{yi}, T_{zi} \end{bmatrix} \\[2ex] \hat{N}_i = \dfrac{m}{|m|} = \begin{bmatrix} N_{xi}, N_{yi}, N_{zi} \end{bmatrix} \\[2ex] \hat{C}_i = \hat{T}_i \times \hat{N}_i = \begin{bmatrix} C_{xi}, C_{yi}, C_{zi} \end{bmatrix} \end{cases}$$

Eq.(3-1)

The normal rake angle γ is measured in the normal plane P_n, which is normal to the cutting edge. The rake face is a continuous surface with a cross sections in the normal plane that consists of the line segment $M_i K_i$, as shown in Fig 3.4.

$\gamma -$ Rake angle

$\sigma -$ Clearance angle

(P_n plane)
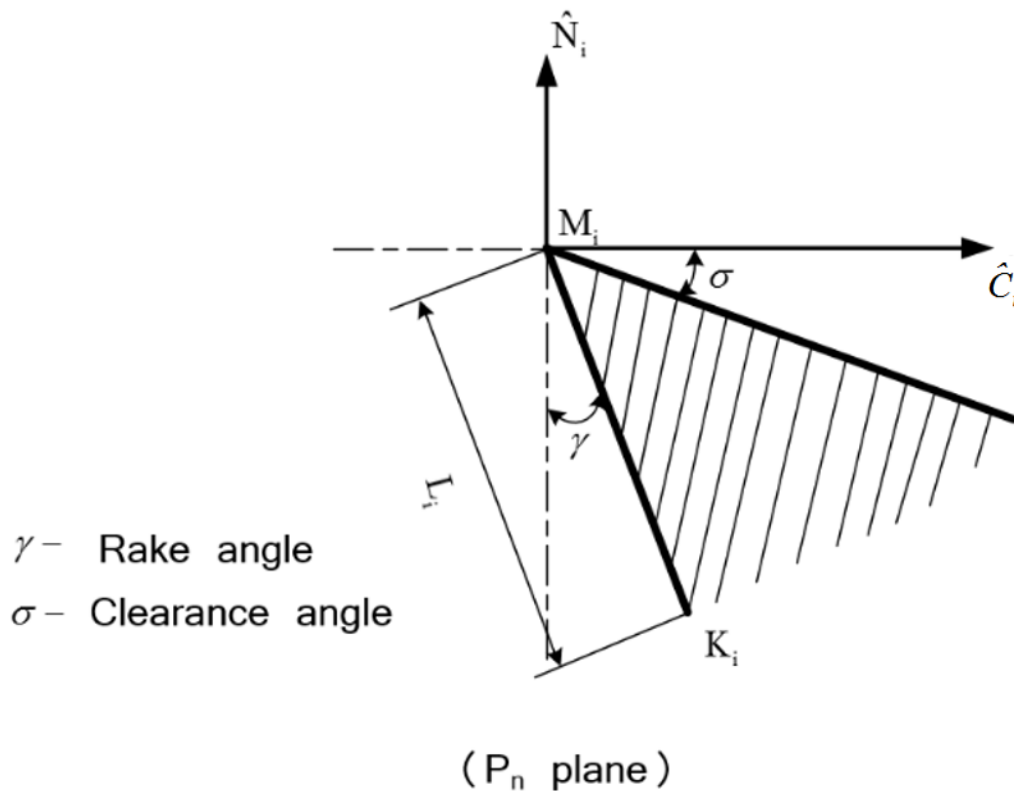
Figure 3.4 Normal Plane of Cutting Edge

For a point on the cutting edge, the depth of cut can be described as M_iK_i, the depth $|M_iK_i| = h_i$ is fixed. It equals zero at the tip and increases in the negative direction of the Z-axis. The highlighted line in red indicates the bottom line of the rake face. The rake face shows in different patterns when the definition differs. As shown in Fig 3.5, it is the model corresponding to the depth $|M_iK_i|$ being described as Eq.(3-2).

$$|M_iK_i| = h_i = (0.25 + 0.15/R) \cdot \sqrt{R^2 - z^2} \text{ where, } 0 \le z \le R \qquad \text{Eq.(3-2)}$$
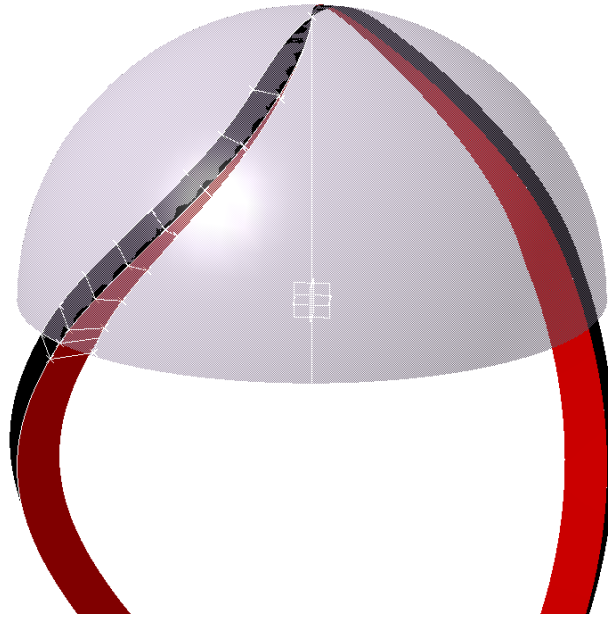
Figure 3.5 Rake Face and Clearance Face Model I

As shown in Fig 3.6, it is the model corresponding to the depth $|M_iK_i|$ being described as Eq.(3-3)

$$|M_iK_i| = h_i = -\frac{h_{max}}{R} \cdot z(\varphi) + h_{max} \qquad \text{Eq.(3-3)}$$
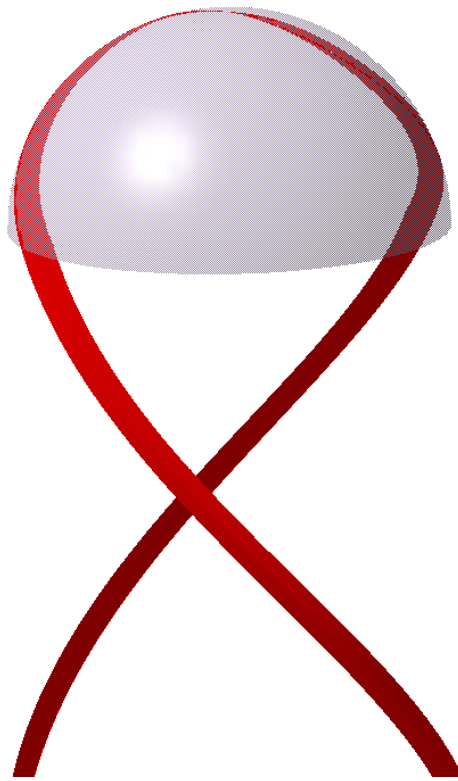
Figure 3.6 Rake Face and Clearance Face Model II

In this case, h_{max} is a assumed parameter that is determined by the user of the modeling software. The relation between $|M_i K_i|$ and $z(\varphi)$ is linear, and h_{max} is the maximum value of the cut depth. Fig 3.7 shows the interface of modifying the h_{max} in Visual Basic.
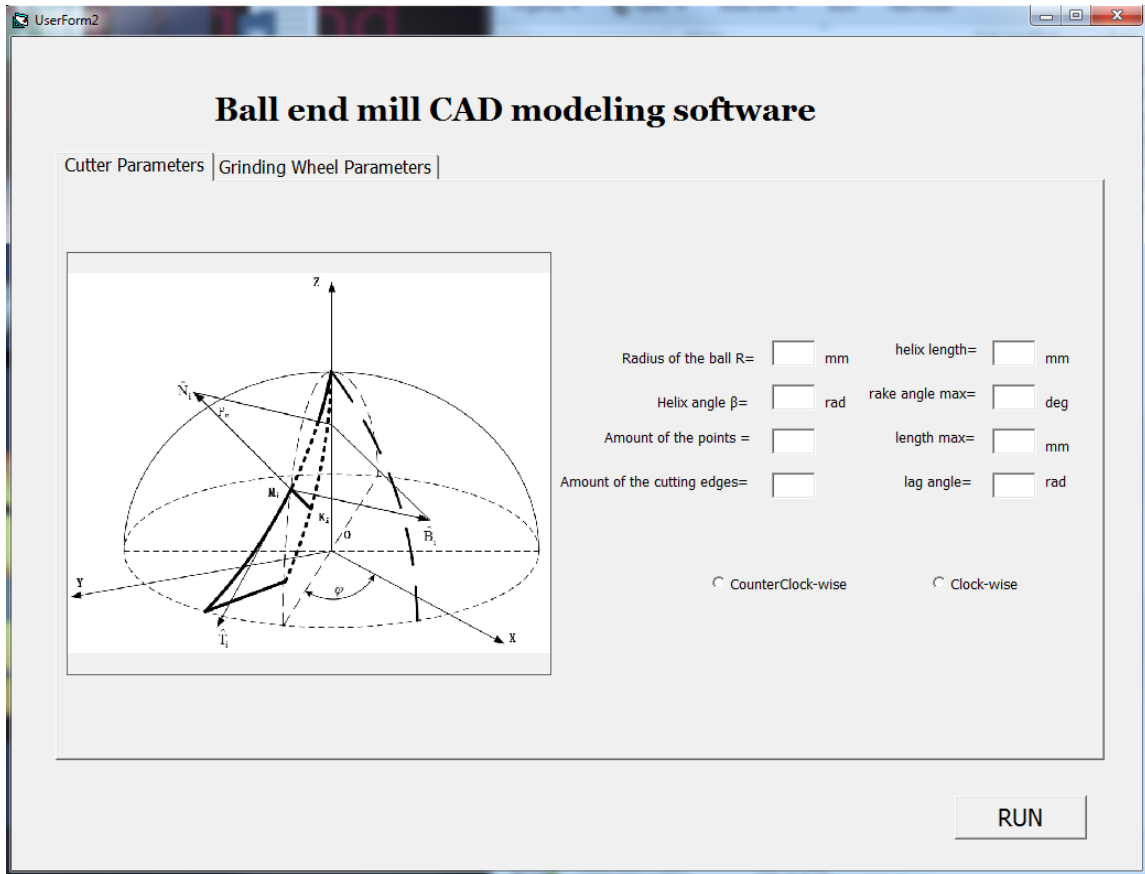
Figure 3.7 Modeling Interface in Visual Basic

3.3.1 Equation for Bottom Curve of rake face

In order to accurately machine the rake face of the ball part with a fixed rake angle and a designed cut depth, the bottom line, which affects the wheel locations, is needed to be determined. in this section, the principle normal vector of the bottom curve and the normal vector of the rake face along the line segment in the normal plane are calculated, which are used in next section to make sure the rake face can be machined without any interference.

The vector of the point K_i on the bottom curve to the point M_i on the cutting edge is indicated in Fig 3.2, and it can be calculated as follow:

$$m_{OK_i} = m_{OC_i} + M_i K_i = [x_{ki}, y_{ki}, z_{ki}] \qquad \text{Eq.(3-4)}$$

Where,

$$\overrightarrow{M_i K_i} = -h_i \cdot cos\gamma \cdot \hat{N}_i - h_i \cdot sin\gamma \cdot \hat{C}_i$$

The bottom curve of the rake face is defined as Eq.(3-4), and it can be parameterized as Eq.(3-5)

$$m_{OK_i} = m_{OK}(\varphi) = [x_k(\varphi), y_k(\varphi), z_k(\varphi)] \qquad \text{Eq.(3-5)}$$

The principle normal vector of the bottom curve of the rake face $\hat{N}_{K_i}$ at point K_i is described as follows, which will be used in next section,

$$\hat{N}_{K_i} = \frac{dm_{OK_i}^2 / d\varphi^2}{\left| dm_{OK_i}^2 / d\varphi^2 \right|} = [N_{K_{xi}}, N_{K_{yi}}, N_{K_{zi}}] \qquad \text{Eq.(3-6)}$$

Therefore, the parameter equation for the rake face based on the equations of the cutting edge and bottom curve can be determined as follows:

$$S(\varphi, \varepsilon) = (1-\varepsilon) \cdot m_{OC_i} + \varepsilon \cdot m_{OK_i} = r_{OC_i} - \varepsilon h_i \left(\hat{N}_i \cdot cos\gamma + \hat{C}_i \cdot sin\gamma \right) \qquad \text{Eq.(3-7)}$$

Where, $0 \le \varepsilon \le 1$

3.3.2 Wheel Locations for Rake Face in Ball Part

In this section, the conditions of engagement between the rake face and grinding wheel are proposed, which can ensure the grinding wheel machining the rake face with its side face precisely avoid interference.

Therefore, the coordinates of the center of the grinding wheel and the vectors of the orientation of the grinding wheel are determined along the cutting edge to machine the rake face of the ball part.

The radius of the grinding wheel is R_w, as shown in Fig 3.8.
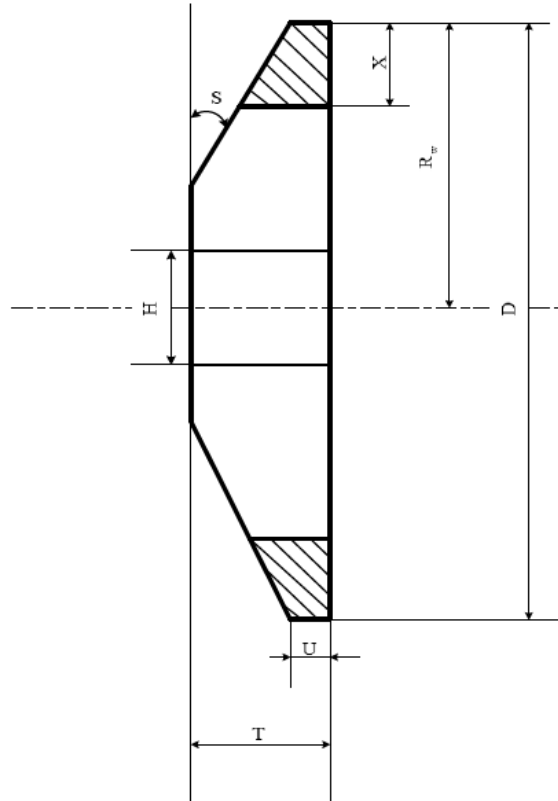
Figure 3.8 Grinding Wheel for Rake Face Sketch

The rake face is machined by grinding each line segment $M_i K_i$, using the side face of the grinding wheel. The side face of the grinding wheel with the center position of G_i, is perpendicular to the wheel axis. In order to avoid interference in machining the rake face with the defined cutting edge, the tangent vector T_i of the cutting edge at the

current grinding point M_i must be coplanar with the side face of the grinding wheel. However, there are many qualified locations of the wheel exist that can realize the line segment M_iK_i can be ground without interference along the cutting edge, as shown in Fig 3.9.
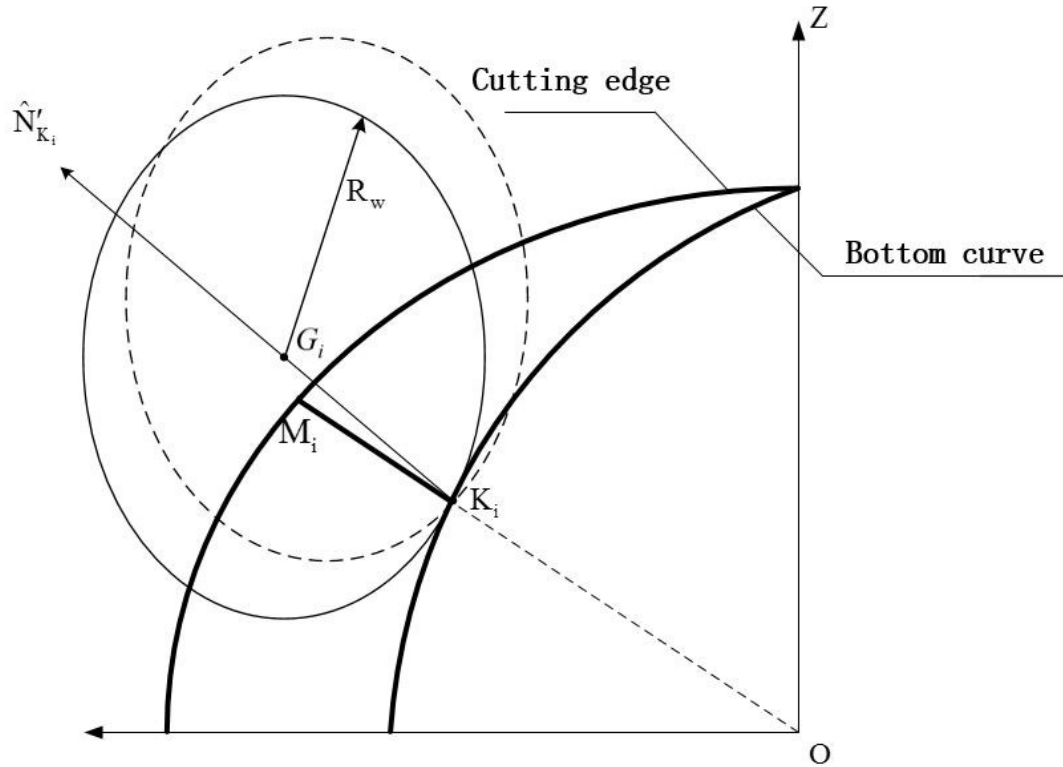
Figure 3.9 Grinding Wheel Interference Situation

However, the grinding wheel at location-1 interferes the defined bottom curve of the rake face. In other words, only the grinding wheel at location-2 can grind the defined rake without any interference. Moreover, to avoid interference between the grinding wheel and the defined bottom curve, the vector $\hat{N}'_{K_i}$ must pass though the center of the grinding wheel side face G_i, as shown in Fig 3.10.
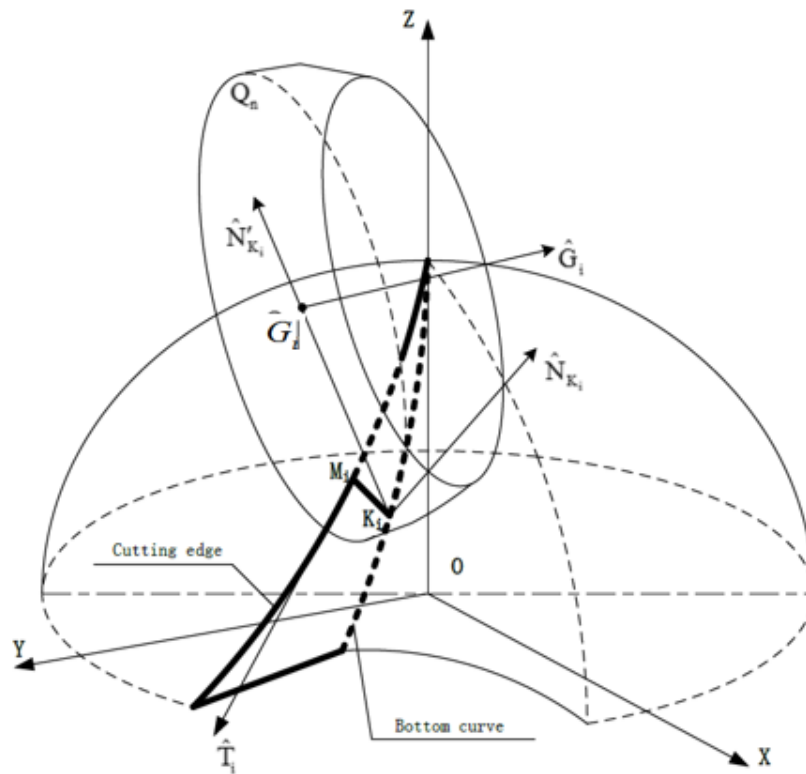
Figure 3.10 Grinding Wheel for Machining Rake Face

The vector $\hat{N}'_{K_i}$ is the projection of the principle normal vector $\hat{N}_{K_i}$ in the plane of the side face of the grinding wheel. The conditions for machining the rake face of the ball part without interference can be described as follows:

1. The line segment $M_i K_i$ must be in the plane of the side face of the grinding wheel. Moreover, the tangent vector of the cutting edge at the grinding point M_i must be contained in the plane of the side face as well.

2. The projection of the principle normal vector $\hat{N}_{K_i}$ of the bottom curve, $\hat{N}'_{K_i}$ must contain the center of the side face of the grinding wheel G_i.

Based on the conditions shown above, the wheel axis $\hat{I}_i$ can be presented as follows:

$$\hat{I}_i = \frac{\hat{T}_i \times K_i M_i}{\left| \hat{T}_i \times K_i M_i \right|} = \left[I_{xi}, I_{yi}, I_{zi} \right]$$
Eq.(3-8)

As the Section 3.3 mentioned,

$$\overrightarrow{M_i K_i} = -h_i \cdot \cos\gamma \cdot \hat{N}_i - h_i \cdot \sin\gamma \cdot \hat{C}_i$$

$$\hat{T}_i = \left[T_{xi}, T_{yi}, T_{zi} \right]$$

Where, $\hat{N}_i = \left[N_{xi}, N_{yi}, N_{zi} \right]$ and $\hat{C}_i = \left[C_{xi}, C_{yi}, C_{zi} \right]$

Therefore, $\overrightarrow{K_i M_i} = h_i \cdot \cos\gamma \cdot \hat{N}_i + h_i \cdot \sin\gamma \cdot \hat{C}_i$, and $\hat{T}_i \times K_i M_i$ can be presented as

follows:

$$\begin{cases} x_{gi} = \hat{T}_{yi} \cdot \left(h_i \cdot \cos\varphi \cdot N_{zi} + h_i \cdot \sin\gamma \cdot C_{zi} \right) - \hat{T}_{zi} \cdot \left(h_i \cos\varphi \cdot N_{yi} + h_i \cdot \sin\gamma \cdot C_{yi} \right) \\ y_{gi} = \hat{T}_{zi} \cdot \left(h_i \cdot \cos\varphi \cdot N_{xi} + h_i \cdot \sin\gamma \cdot C_{xi} \right) - \hat{T}_{xi} \cdot \left(h_i \cos\varphi \cdot N_{zi} + h_i \cdot \sin\gamma \cdot C_{zi} \right) \\ z_{gi} = \hat{T}_{xi} \cdot \left(h_i \cdot \cos\varphi \cdot N_{yi} + h_i \cdot \sin\gamma \cdot C_{yi} \right) - \hat{T}_{yi} \cdot \left(h_i \cos\varphi \cdot N_{xi} + h_i \cdot \sin\gamma \cdot C_{xi} \right) \end{cases}$$

On the basis of the conditions1 and conditions 2 above, the position of the wheel center

is determined by Eq.(3-10)

$$m_{OG_i} = m_{OK_i} + \hat{N}'_{K_i} \cdot R_w$$
Eq.(3-10)

There is only one common point K_i between the grinding wheel and the bottom curve

of the rake face. And we can get the conclusion from the conditions above that I_i and

$\hat{N}_{K_i}$, these two vectors are intersected, thus, I_i, $\hat{N}_{K_i}$ and $\hat{N}'_{K_i}$ are coplanar. The vector

$\hat{N}'_{K_i}$ can be obtained as follows:

$$\hat{N}'_{K_i} = \frac{\left(\hat{I}_i \times \hat{N}_{K_i} \right) \times \hat{I}_i}{\left| \left(\hat{I}_i \times \hat{N}_{K_i} \right) \times \hat{I}_i \right|}$$
Eq.(3-11)

When the side face of the grinding wheel contains the line segment $M_i K_i$, the wheel axis orientation is defined to be equivalent to the normal of the rake face at the grinding point M_i. Then the contact line between the designed rake face and the side face of the grinding wheel is this line segment. The position of the wheel center and the orientation of wheel axis that are required for accurate machining of the rake face are determined by Eq.(3-10) and (3-8), respectively. Moreover, Eq.(3-12) is to prove the normal of the rake face is constant along the line segment $M_i K_i$.

$$
I_i = \frac{\dfrac{\partial S(\varphi,\varepsilon)}{\partial \varphi} \times \dfrac{\partial S(\varphi,\varepsilon)}{\partial \varepsilon}}{\left| \dfrac{\partial S(\varphi,\varepsilon)}{\partial \varphi} \times \dfrac{\partial S(\varphi,\varepsilon)}{\partial \varepsilon} \right|}
$$

$$
= \frac{\left| \dot{m} \left| \hat{T}_i - \varepsilon h_i \left(\dfrac{|\dot{m}|}{R} cos\gamma \cdot \hat{T}_i + k_n \sin\gamma \cdot \left(\hat{N}_i \times \hat{N}_{Fi} \right) \right) \right| \times \left(-h_i \left(cos\gamma \cdot \hat{N}_i + sin\gamma \cdot \hat{C}_i \right) \right)}{\left\| \left(|\dot{m}| - \varepsilon h_i \left(\dfrac{|\dot{m}|}{R} cos\gamma + k_n sin\gamma \cdot sin\psi \right) \right) \cdot h_i \right\|}
\qquad \text{Eq.(3-12)}
$$

$$
= cos\gamma \cdot \hat{C}_i - sin\gamma \cdot \hat{N}_i
$$

Where, $\hat{N}_{Fi}$ is the principle normal vector, k_n is the normal curvature, and ψ is the angle between the principle normal vector $\hat{N}_{Fi}$ and the normal of the sphere $\hat{N}_i$ at the current grinding point M_i.

Fig 3.11 shows the grinding status in CATIA, the volume in blue represents the grinding wheel, and the other volume is the tool bar. The grinding wheel is machining the tool bar and the wheel side face profile is tangent to the bottom curve of the rake face.
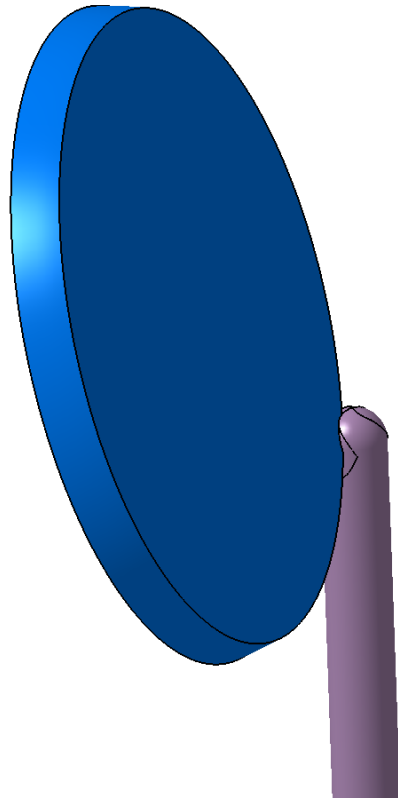
Figure 3.11 Grinding Rake Face View in CATIA

3.4 Mathematical Model for Clearance Face in Ball Part

In machining process, the clearance angle of the ball end mill affects the cutting force, chips removal and some other conditions which significantly determines the cutting performance and the tool life. Moreover, the clearance face shape is an

important component of a ball end mill, and it can be different prior to the grinding method.

In this paper, the first and second clearance face calculation will be presented in this section. And the clearance face and clearance angle definition is shown in Fig 3.12.
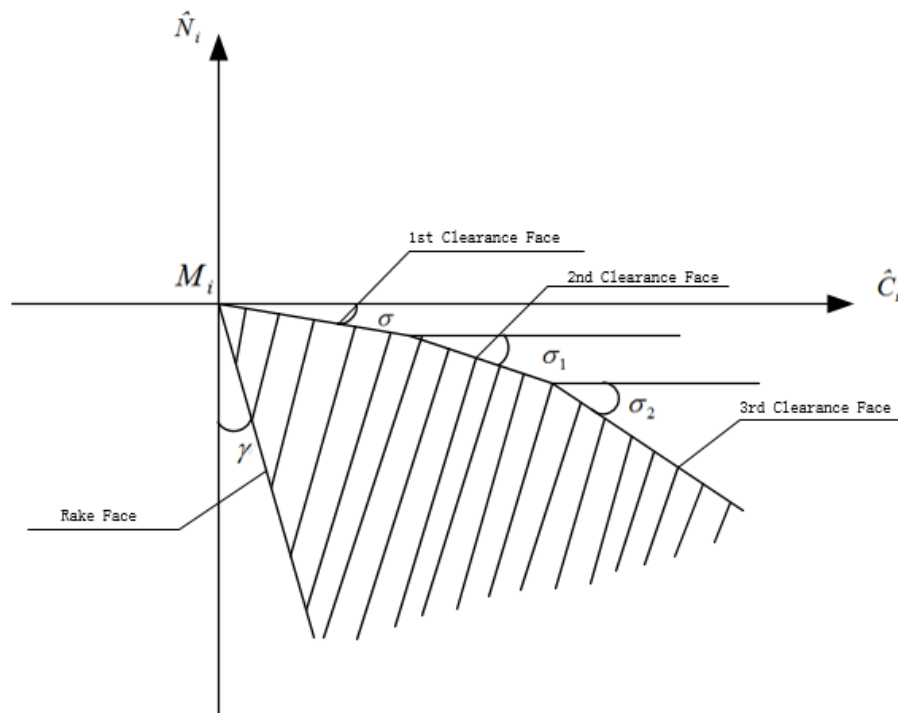
Figure 3.12 Clearance Face View in Normal Plane

The clearance angle σ, is defined as the angle between the tangent vector at point M_i and the direction of the vector $\hat{C}_i$ in the normal plane. The clearance face is machined by the outer circle face of the grinding wheel in the concave method and by the side face of the grinding wheel in the flat method. The parameters of the grinding

wheel for the clearance face are shown in Fig 3.13:
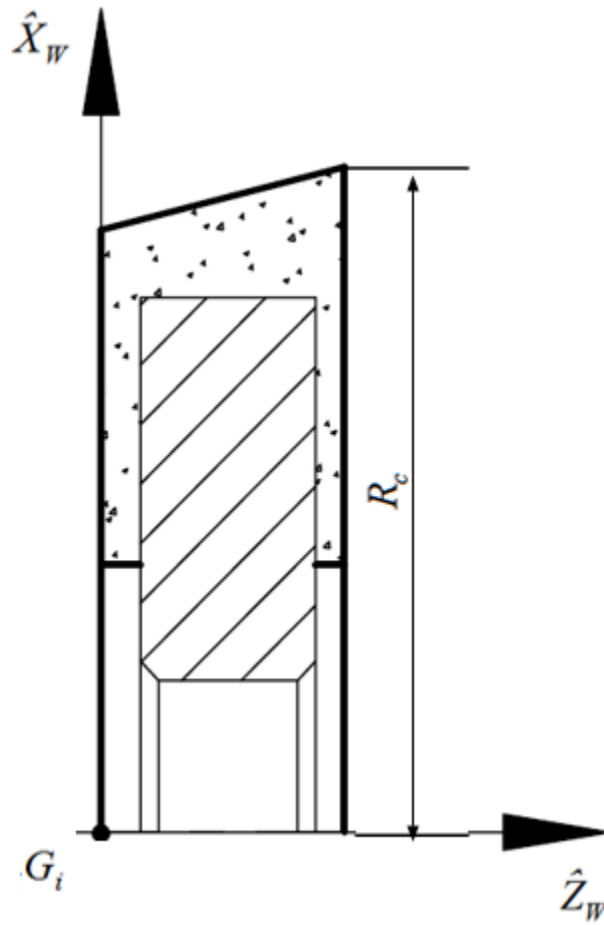
Figure 3.13 Grinding Wheel for Clearance Face Sketch

3.4.1 Construction of the Clearance Face in Concave method

In this section, the grinding wheel location can be determined by the cutting edge

and its basic components. Once the grinding wheel center position and axis orientation

are calculated, the concave-shape clearance face with a constant clearance angle can be

obtained along the cutting edge.

The location of the grinding wheel for machining the concave-shape clearance face is shown in Fig 3.14 and Fig 3.15. The clearance face is formed by the circle face of the grinding wheel, and the axis of the grinding wheel is perpendicular with the tangent vector of the cutting edge. Moreover, to ensure the clearance angle σ being constant, the tangent vector of the grinding wheel outer circle at the grinding point M_i make a angle of the value of clearance angle with the direction of $\hat{C}_i$.

Therefore, the relative position of the grinding wheel center and the orientation of wheel axis are determined as follows:

$$m_{OG_i} = m_{OM_i} + M_i G_i \qquad\qquad \text{Eq.(3-13)}$$

Where, $M_i G_i = R_c \cdot \left(sin\sigma \cdot \hat{C}_i + cos\sigma \cdot \hat{N}_i \right)$

The orientation of the wheel axis can be presented as follows:

$$\hat{I}_i = \hat{C}_i \times \hat{N}_i \qquad\qquad \text{Eq.(3-14)}$$
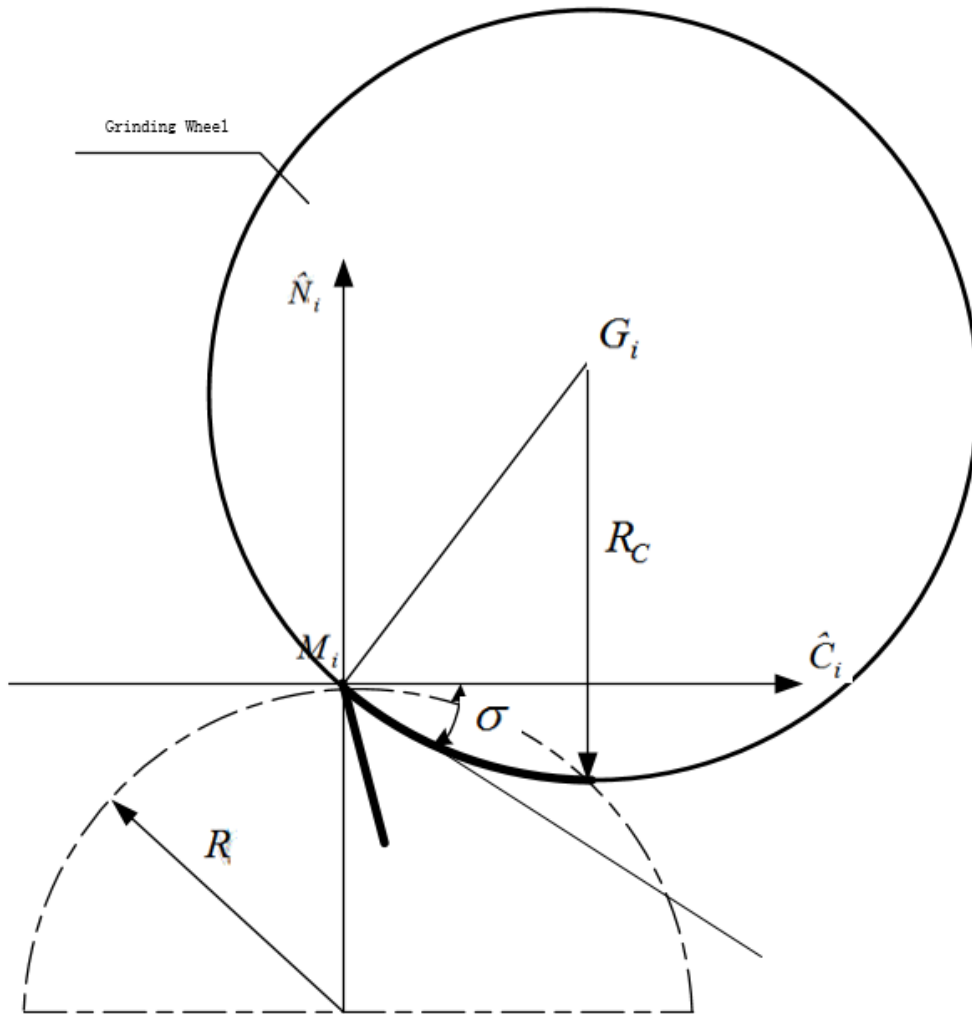
Figure 3.14 Axis Cross Section View of the Grinding Wheel
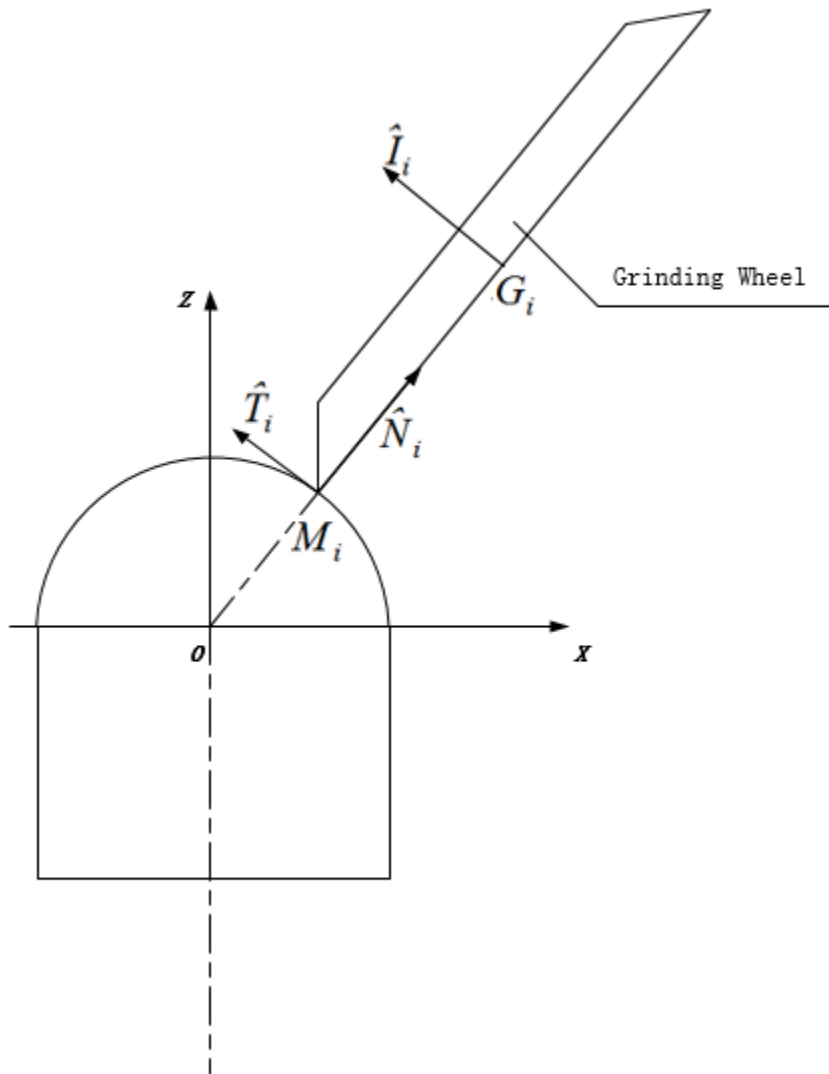
Figure 3.15 x-o-z Plane View of Grinding Concave Clearance Face

3.4.2 Construction of the Clearance Face in Flat method

In this section, the grinding wheel location can be determined by the cutting edge and its basic components. Once the grinding wheel center position and axis orientation

are calculated, the concave-shape clearance face with a constant clearance angle can be obtained along the cutting edge.

The model for grinding flat-shape clearance face is shown in Fig 3.16. The clearance face is machined by the side face of the grinding wheel moving along the cutting edge. The orientation of the wheel axis makes a angle of the value of the clearance angle. The grinding wheel intersects the ball part at each grinding point, and that intersection presents as a line segment. The length of this line segment is defined as the width of the clearance face.

Therefore, the position of the center of the grinding wheel is obtained as follows:

$$m_{OG_i} = m_{OM_i} + M_i G_i \qquad\qquad\text{Eq.(3-15)}$$

Where, $M_i G_i = R \cdot sin\,\sigma \cdot \left(cos\,\sigma \cdot \hat{C}_i - sin\,\sigma \cdot \hat{N}_i\right) - \sqrt{R_c^2 - (R \cdot sin\,\sigma)^2} \cdot \hat{T}_i$

The orientation of the grinding wheel axis can be calculated as follows:

$$\hat{I}_i = cos\,\sigma \cdot \hat{N}_i + sin\,\sigma \cdot \hat{C}_i \qquad\qquad\text{Eq.(3-16)}$$
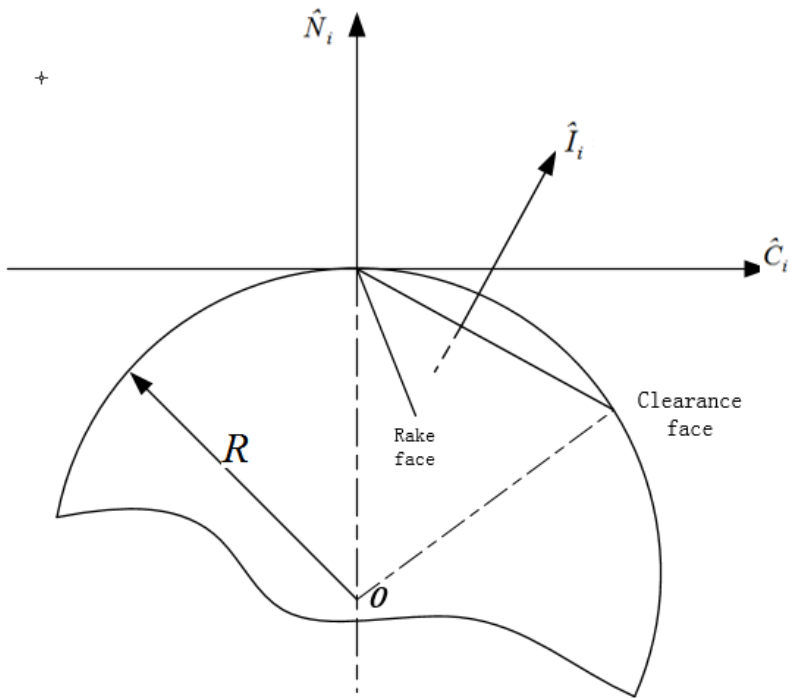
Figure 3.16 Grinding Wheel Axis Orientation
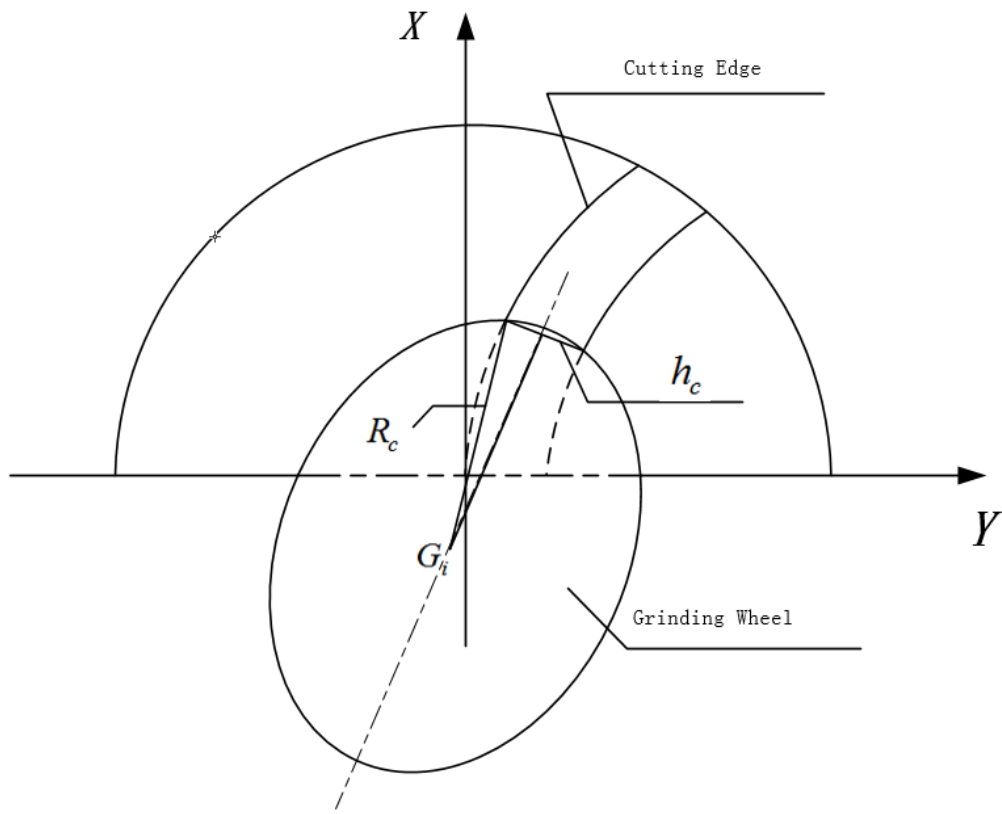
Figure 3.17 Wheel Center Location of Flat-shaped Clearance Face

3.5 Calculation Results Applied in Matlab and CATIA

The mathematical model of the cutting edge, rake face, and clearance face are built in last several sections. Our goal is to create the 3D model in CATIA, and then the analysis and simulations work can be done. Therefore, building a bridge between the mathematical equations and the software is definitely important.

First of all, the equations require to be imported to MATLAB. Once the program is

created, several parameters need to be fixed to calculate the data. Table 3-1 shows the parameters that need to be set before the calculation in MATLAB.

Table 1-1 Parameter Setting for Rake face

	Setting Values
Radius of ball	6mm
Helix angle	57 degrees
Number of the discrete points	80
Number of flutes	2
Helix length	80mm
Rake angle max	3 degrees
Width max	1.85mm

Table 1-2 Parameters of the Grinding Wheel for Rake Face

	Setting Values
1st Radius Rw	56.45mm
2nd Radius Rc	58.76mm
Width L	7.6mm

Table 1-3 Parameters of the Grinding Wheel for Clearance Face

	Setting Values
1st Radius Rw	57.1mm
2nd Radius Rc	59mm
Width L	8.5mm

With the calculation in MATLAB, we can code the program to produce the ".txt" file in specified folder. The data in this file will be specified amount of coordinates. These coordinates can be applied in VB program to control CATIA creating points. For the cutting edge of the ball part, the dissociated points can be connected as a spline in CATIA, which is the way to obtain the cutting edge curve. In terms of the grinding wheel location, the data produced by MATLAB indicates the dissociated center points of the grinding wheels at each locations, and the orientations of the axis of the grinding wheel.

Table 3-2 and Table 3-3 shows the parameters of the grinding wheels for machining the rake face and clearance face, respectively.

Chapter 4. Design and Modeling of Flute Surface

4.1 Introduction

After the equation of the cutting edge and the normal rake angle and clearance angle are given, with the cut depth is set in the program, the rake face can be modeled in CATIA. Meanwhile, the positions of the grinding wheel center and the orientations of the grinding wheel axis are calculated in MATLAB in previous sections, which makes it possible to obtain the flute surface of the ball part. However, this surface is ground by the revolution surface of the grinding wheel.

In this section, the generated surface of the flute will be calculated with the goal of visualization and simulation. The flute surface is calculated by the tangency condition at each grinding point of the wheel surface.

The flute surface is important for a ball end mil, because it determines the cutting performance and the chip removal. Although it is possible to obtain the flute surface by Boolean operation in commercial software, for the precise simulation purpose, it is required to present a direct calculation of the surface.

4.2 Calculation of the Flute Surface

The flute surface is determined by enveloping the surface of the moving grinding wheel along the cutting edge. And it consists of three factors:

1. The surface of the grinding wheel at the starting position.

2. Swept surface of the moving grinding wheel.

3. The surface of the grinding wheel at the final position.

Wheel Moving

t=0

t=t

$$N_I \cdot V_I < 0$$

$$N_I \cdot V_I = 0$$

$$N_I \cdot V_I > 0$$
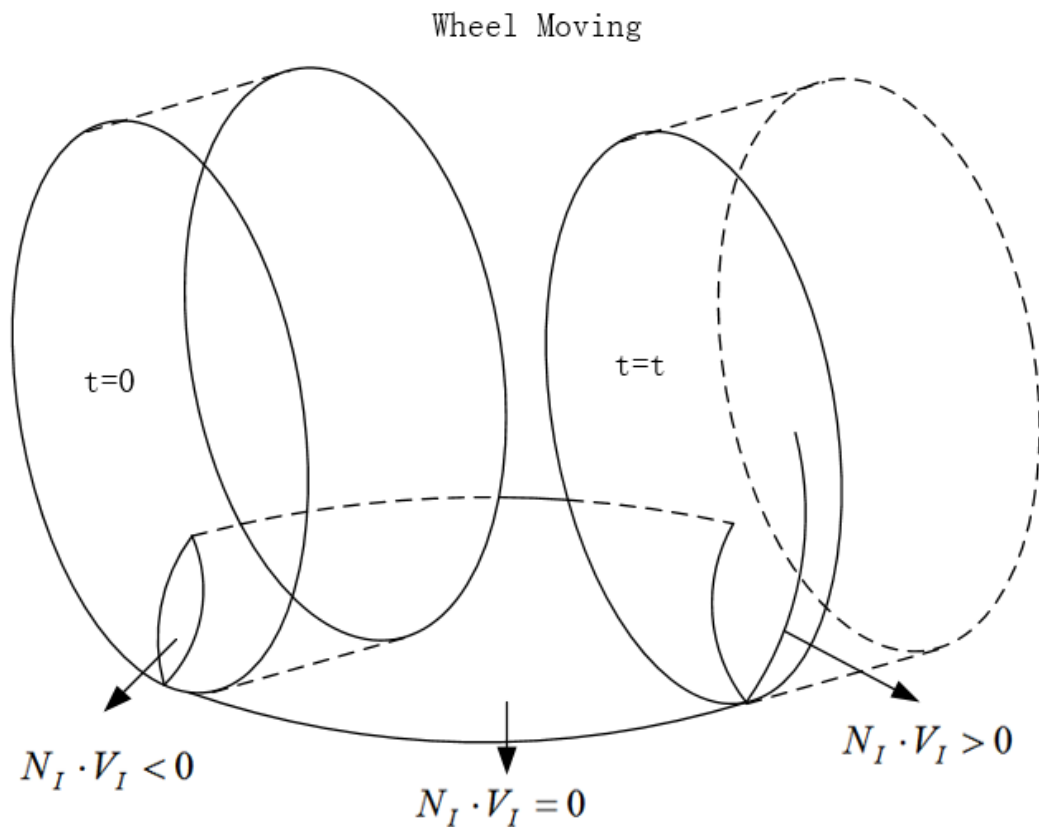
Figure 4.1 Generated Surface by the Moving Wheel

The points on the swept surface are determined by an important condition, which is

the grinding wheel is always tangent to the swept envelope along a sweeping profile, as shown in Fig. 4.1. Thus, the unit normal vector N_I, is parallel to the vector normal to the swept surface at any point I on the swept surface. Moreover, the velocity vector V_I, of point I is constrained to be tangent to the swept surface. Therefore, the swept surface can be determined based on the tangency condition as follows:

$$N_I \cdot V_I = 0 \qquad \text{Eq.(4-1)}$$

But the rear surface and the front surface are parts of the flute surface as well, in this case, the conditions shown as follows will be applied:

For rear surface,

$$N_I \cdot V_I < 0 \qquad \text{Eq.(4-2)}$$

For front surface,

$$N_I \cdot V_I > 0 \qquad \text{Eq.(4-3)}$$

The wheel location center trajectory calculated in previous section can be parameterized as follows:

$$m_G(t) = \left(m_{OG_{xi}}, m_{OG_{yi}}, m_{OG_{zi}} \right) \qquad \text{Eq.(4-4)}$$

And the unit vector of the orientation of the wheel axis can be parameterized as follows:

$$\hat{I}(t) = \left(I_{xi}, I_{yi}, I_{zi} \right) \qquad \text{Eq.(4-5)}$$

Therefore, the movement of the grinding wheel can be determined by the trajectory the wheel center locations $m_G(t)$, and the wheel axis orientation is given. A coordinate system of the grinding wheel can be founded at the wheel center, which is presented as

follows:

$$\begin{cases} \hat{X}_W = \dfrac{\dot{i}}{|\dot{i}|} \\ \hat{Y}_W = \hat{Z}_W \times \hat{X}_W \\ \hat{Z}_W = \hat{I} \end{cases}$$

Eq.(4-6)

Fig 4.2 indicates the coordinate system visually.
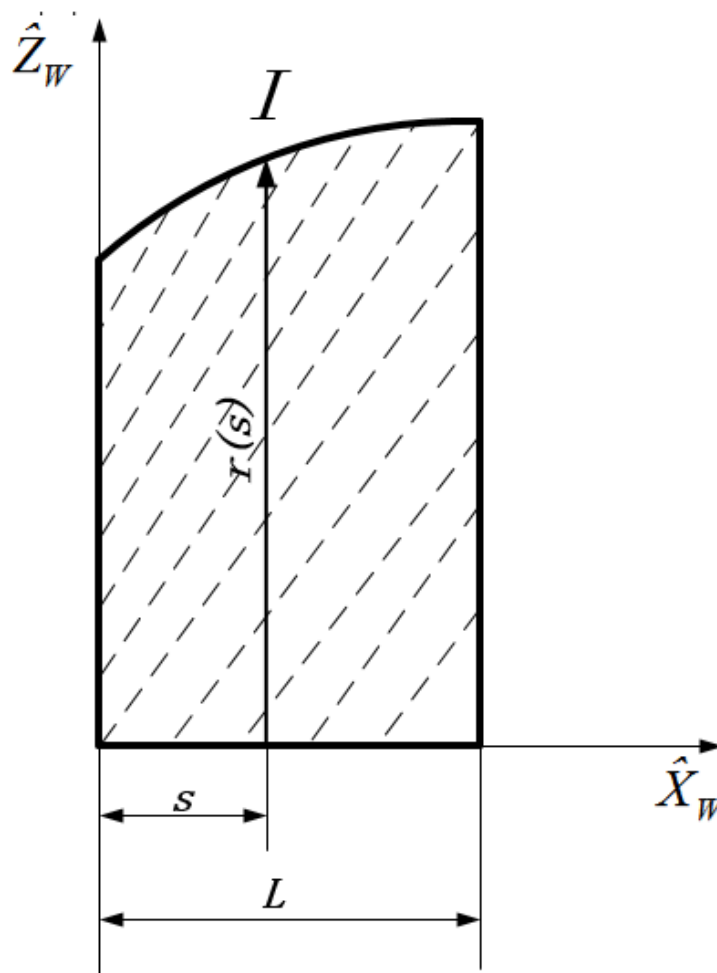
Figure 4.2 Grinding Wheel Coordinate System

The axial cross-section of the grinding wheel with the width, L, in the $X_W Z_W$ plane

of the grinding wheel coordinate system is created in Fig. 4.3. The parametric equations

of the revolution surface of the wheel can be obtained by rotating a curve along the Z_W-

axis, and it can be presented as follows:

$$S_W(s,\theta,t) = m_G(t) + r(s) \cdot \cos\theta \cdot \hat{X}_W + r(s) \cdot \sin\theta \cdot \hat{Y}_W + s \cdot \hat{Z}_W \qquad \text{Eq.(4-7)}$$

Here, the normal vector N_I and the velocity vector V_I are required to be calculated.

In the cross-section of the wheel surface which normal to the wheel axis $\hat{I}$, offset from

the wheel center a distance s in the Z_W axis, taking a point I in that cross-section at an

angle, θ, measured from the axis X_L. The velocity of point I and the normal of wheel

surface at point I are determined in workpiece coordinates as follows:
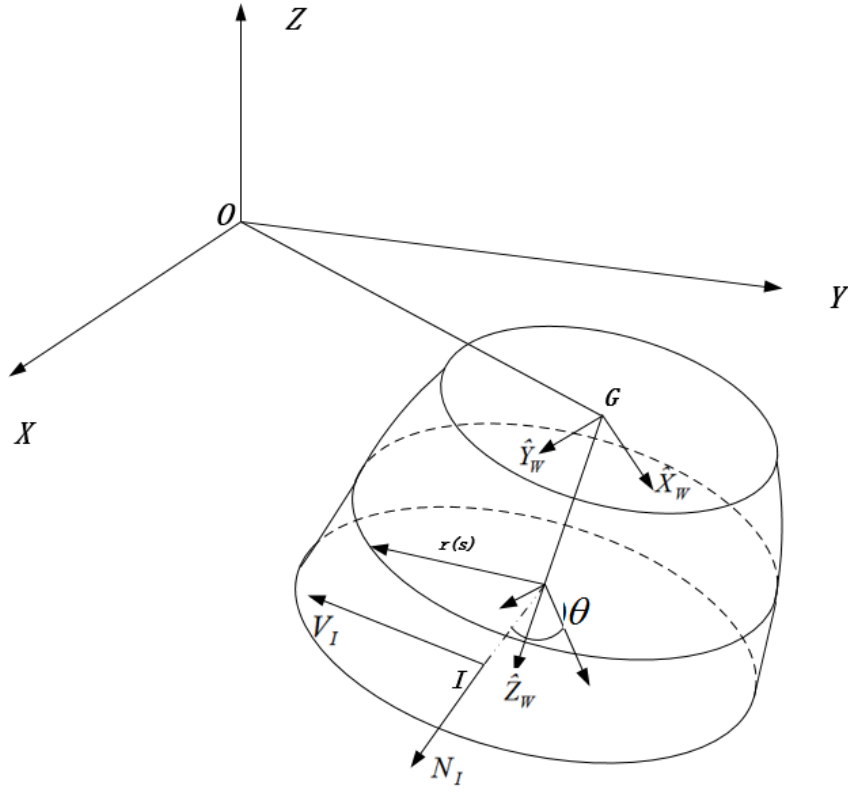
Figure 4.3 Grinding Wheel Coordinate System

$$V_I = \omega_G \times r_{GI} + V(G)$$
$$= \left|\hat{I}\right| \cdot \hat{Y}_W \times \left(r(s) \cdot \cos\theta \cdot \hat{X}_W + r(s) \cdot \sin\theta \cdot \hat{Y}_W + s \cdot \hat{Z}_W\right) + \dot{m}_G \qquad \text{Eq.(4-8)}$$

Where, ω_G is the instant angle velocity of the wheel.

Therefore, the velocity vector V_I can be simplified as follows:

$$V_I = \dot{m}_G + s \cdot \left|\hat{I}\right| \cdot \hat{X}_W - \left|\hat{I}\right| \cdot r(s) \cdot \cos\theta \cdot \hat{Z}_W \qquad \text{Eq.(4-9)}$$

Moreover, the normal vector of the wheel surface at general point I can be calculated

as follows:

$$N_I = \cfrac{\cfrac{\partial S_W(s,\theta,t)}{\partial \theta} \times \cfrac{\partial S_W(s,\theta,t)}{\partial s}}{\left| \cfrac{\partial S_W(s,\theta,t)}{\partial \theta} \times \cfrac{\partial S_W(s,\theta,t)}{\partial s} \right|}$$

$$= \frac{\cos\theta \cdot \hat{X}_W + \sin\theta \cdot \hat{Y}_W - \dot{r}(s) \cdot \hat{Z}_W}{\sqrt{1 + \dot{r}^2(s)}}$$

Eq.(4-10)

For the swept surface of the moving wheel, $N_I \cdot V_I = 0$, we can get the following equation:

$$\left(\dot{m}_G \cdot \hat{X}_W + |\dot{i}| \cdot r(s) \cdot \dot{r}(s) + |\dot{i}| \cdot s \right) \cdot \cos\theta + \dot{m}_G \cdot \hat{Y}_W \cdot \sin\theta - \dot{r}(s) \cdot \dot{m}_G \cdot \hat{Z}_W = 0$$

Eq.(4-11)

Therefore, we can obtain the contact line between the grinding wheel surface and the swept surface. For the case of the initial position and final position, as stated previously, the condition $N_I \cdot V_I < 0$ and $N_I \cdot V_I > 0$ must be satisfied, respectively.

Above all, the flute surface machined by the moving grinding wheel can be determined.

4.3 Flute Surface Construction in CATIA

4.3.1 Flute Surface in Ball Part

After the Boolean operation for the grinding wheel and ball part workpiece, the flute surface can be obtained. But the surface is shown hackly in CATIA because of the disadvantage of Boolean operation. Even though, we can calculate the wheel locations intensively in MATLAB, the surface is not smooth enough. Here, we will show the operation method to obtain a smooth flute surface.

At each location, the grinding wheel intersects the workpiece as a contact curve. The intersection can be easily obtained in CATIA with the function "intersection". In geometric shape design, we can use the function "multi-section surface" to connect these contact line to a surface. Thus, by splitting the workpiece with the multi-section surface, the smooth flute surface can be obtained, as shown in Fig 4.4.
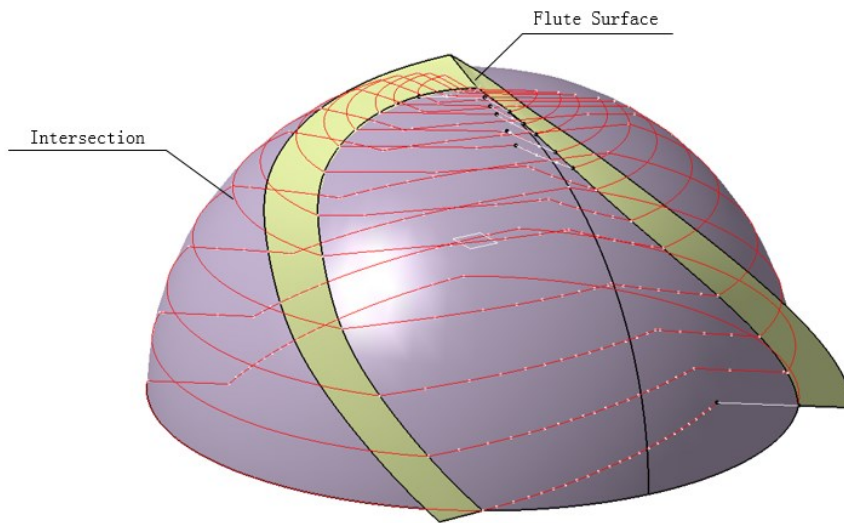
Figure 4.4 Flute Surface Split

It can be also applied to the clearance surface, as shown in Fig 4.5.
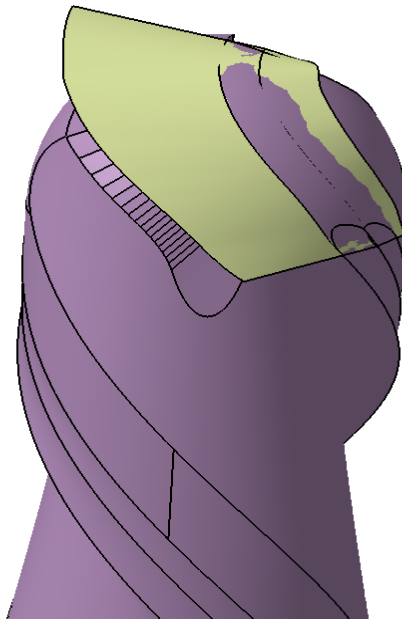
Figure 4.5 Clearance Face Surface

4.3.2 Flute Surface in Cylinder Part

For the flute surface in cylinder part, we take the method in the thesis "A New CAD/CAM/CAE Integration Approach to Modeling Flutes of Solid End-mills". By calculating the coordinates of the points in the axial cross-section of the toolbar, the points can be obtained in CATIA as shown in Fig 4.6.
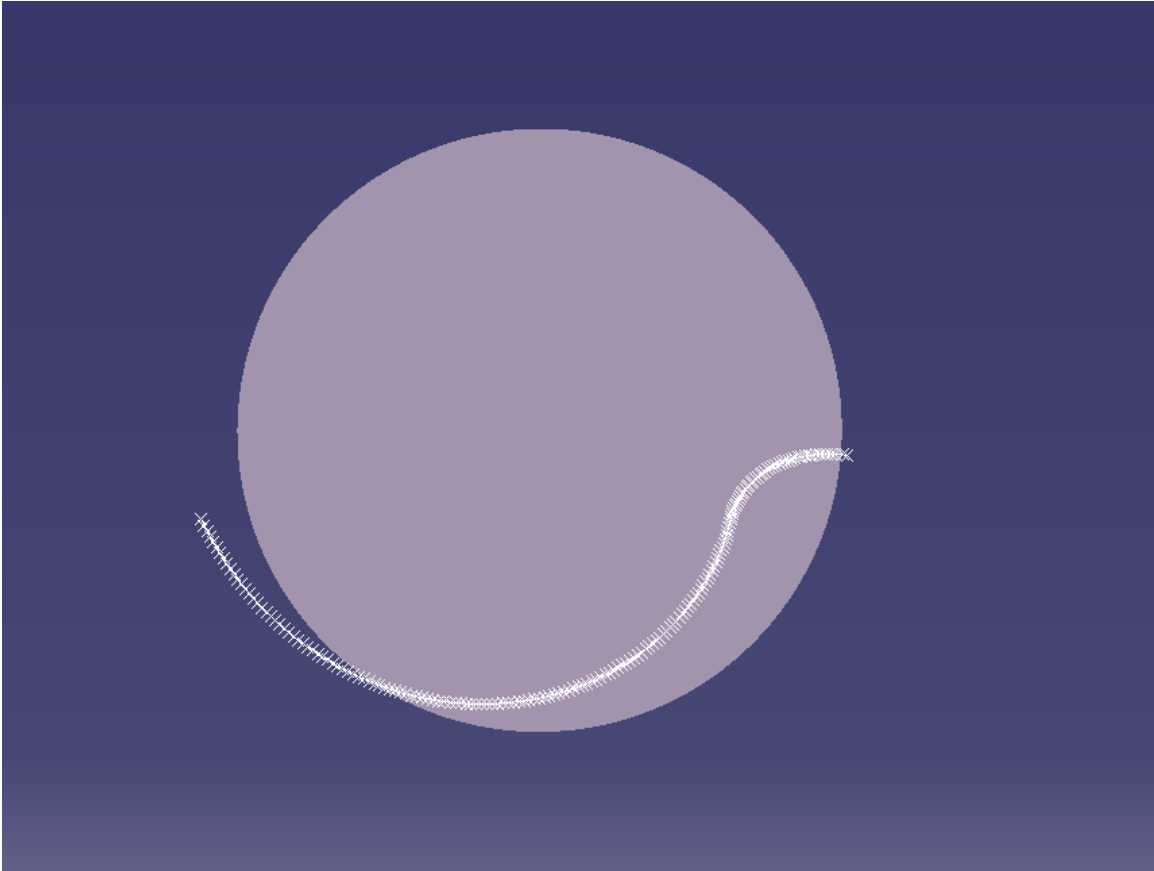
Figure 4.6 Flute Profile on Cylinder Part

By using the "spline" function, all of the points can be connected to a spline curve, which is defined as the object to be swept. As stated previously, the helix angle and radius of the toolbar has been defined. Therefore, we can obtain the flute surface by sweeping the spline curve shown in Fig 4.7 along the helix, as shown in Fig 4.8.
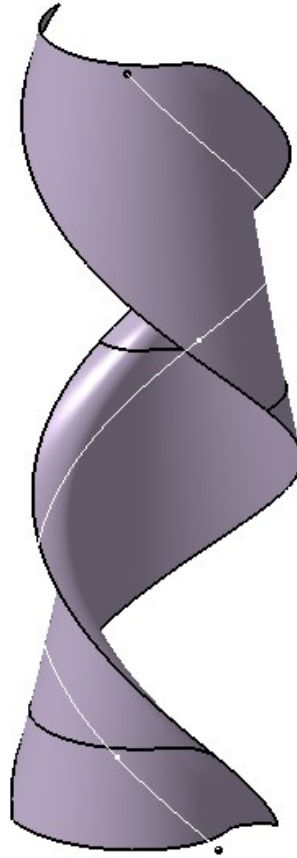
Figure 4.7 Flute Surface based on sweeping the Flute Profile along Helix
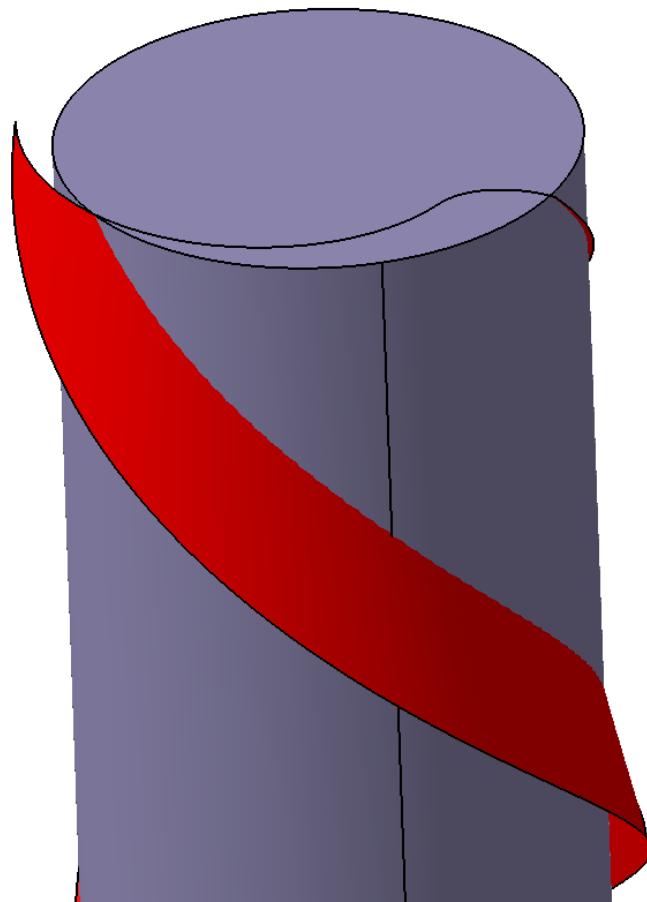
Figure 4.8 Modeling the Flute surface with Flute Profile

Chapter 5. APPLICATION

5.1 Introduction of the Commercial Simulation Software

The modeling process of ball end mill and flute surface is demonstrated in two chapters previously. By gathering all of the modeling features, the whole ball end mill can be built in 3D modeling commercial software, i.e. CATIA, SOLIDWORKS etc. In this paper, we apply all the modeling work in CATIA. To verify the design standard and performance of the model, it is required to conduct a simulation in a software. FEA technique is widely used in many simulation software. Finite element analysis can obtain approximate solutions to engineering simulation problems which transfers a whole part into simpler parts to get a close result.

Third Wave Advantedge is a software for optimization of metal cutting with validated finite element technique to analyze machining processes in 2D and 3D environments. The model of ball end mill in CATIA can be imported into Advantedge for further analysis. By defining geometries and materials of tools and workpiece, in addition, setting the cutting conditions, the results of cutting process are generated, such as: temperature, stress, chip formation and power consumption. The interface of the Third Wave Advantedge is shown in Fig 5.1.
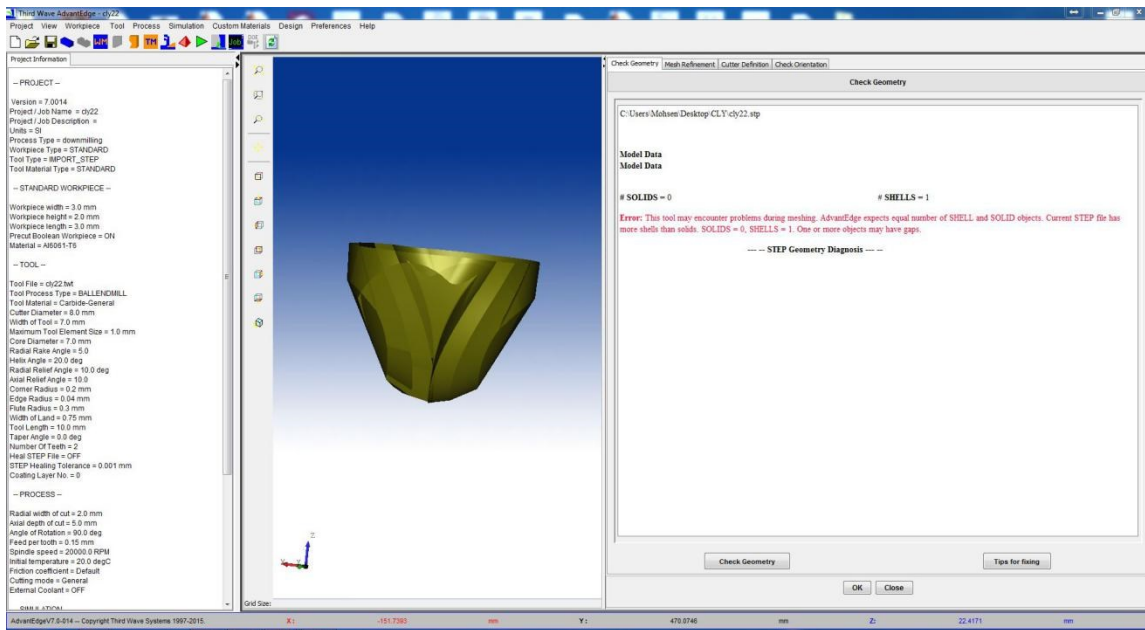
Figure 5.1 Third Wave AdvantEdge Interface

5.2 Basic Settings in Third Wave AdvantEdge

5.2.1 Tools and Workpiece Material

Cutting tools are mostly operated at high temperature and under heavy loads. Several major requirements for cutting tools are: good physical and chemical properties under high temperature, especially hot-hardness. High wear resistance and high resistance to brittle fracture [24]. However, single material cannot satisfy all of the properties. For instance, if the high-temperature resistance and wear resistance of a kind of material are high, the resistance to brittle fracture will probably be reduced.

Most kinds of tool material in industry are carbon steels, high-speed steels, cast

alloys, cemented carbide and ceramics. Cemented carbides is the kind of the most widely used material in industry. Cemented carbides varies three categories: P, M and K. As shown in Fig 5.2. Cemented carbides P deals with material that produce long chips, including most steels; M for stainless and heat resistant alloys; K for cast irons, nonferrous alloys and hardened steels. In Third Wave Advantedge software, all types of carbide are provided. Carbide-Grade-M is selected as the material of the ball end-mill, because end mills are always used for multiple purposes.
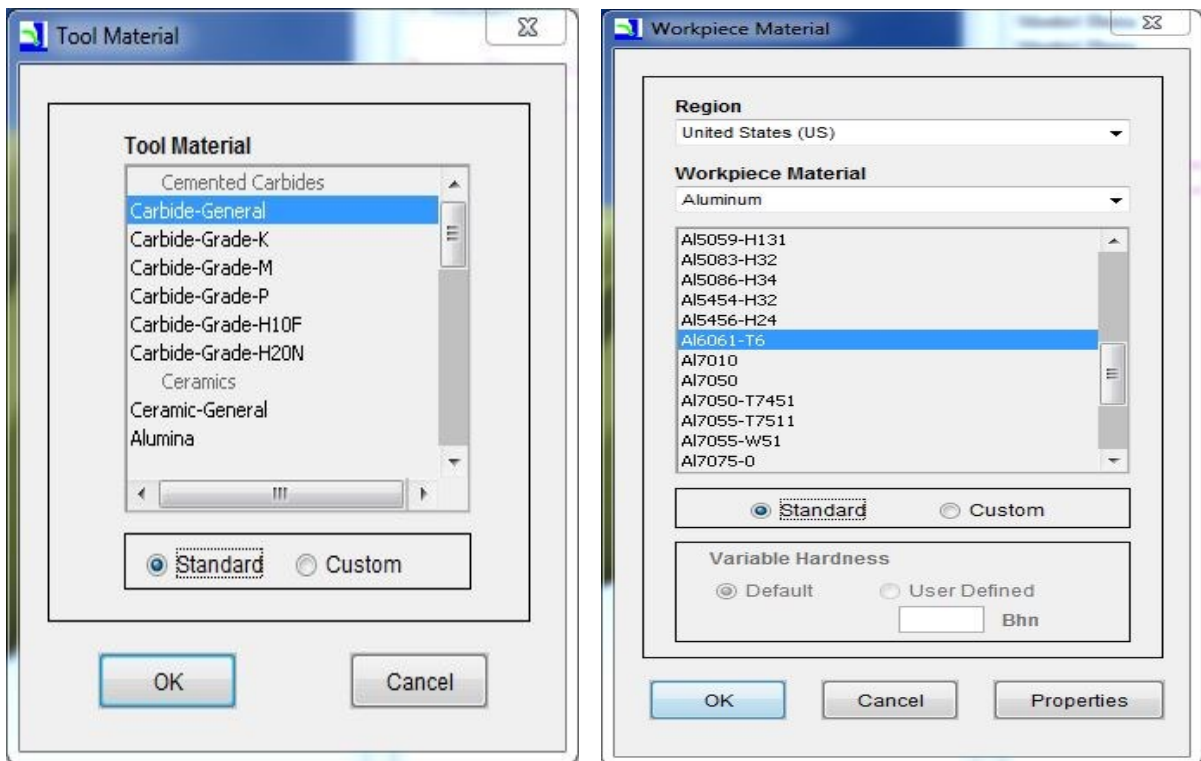
Figure 5.2 Material Selection of Tools and Workpiece

In Advantedge, various workpiece materials are available. As titanium alloy is one of the most high performance metals with high tensile strength and toughness, it is

preferable for simulation which could give contrasting results. Titanium alloy are divided

into numbers of categories among which Grade 5(Ti-6Al-4V) is the most frequently used
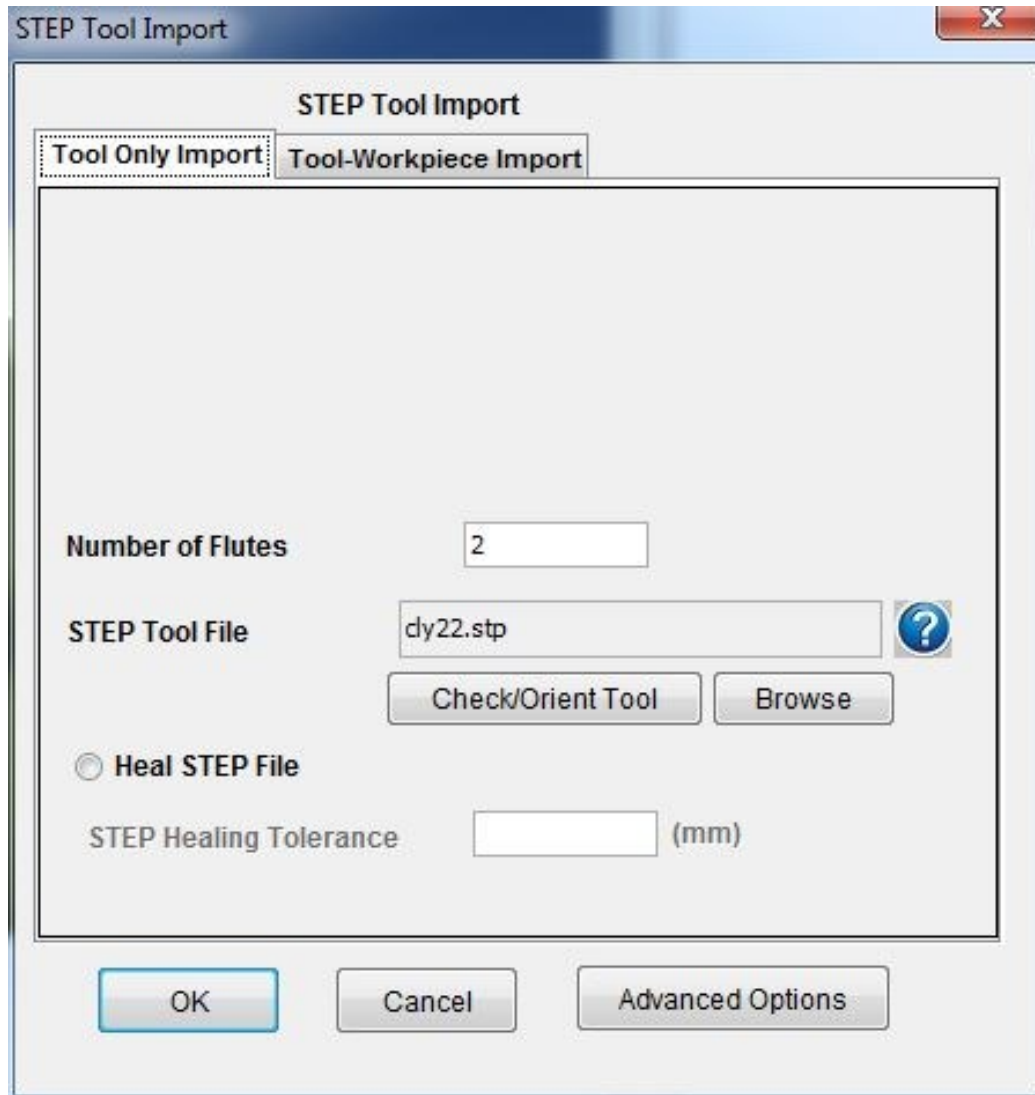
Figure 5.3 Import the 3D Model of the Tool

kind of alloy. So Ti-6Al-4V is set as the material of the workpiece in the simulation.

After determining the materials of the tools and workpiece, we can import the

cutter to the software as shown in Fig 5.3. For the reason of that FEA is a time

consuming work, if the entire cutter were imported, there would be too much useless calculation process. Therefore, we will select part of the tool as the model which is imported to the software for simulation as shown in Fig 5.4.
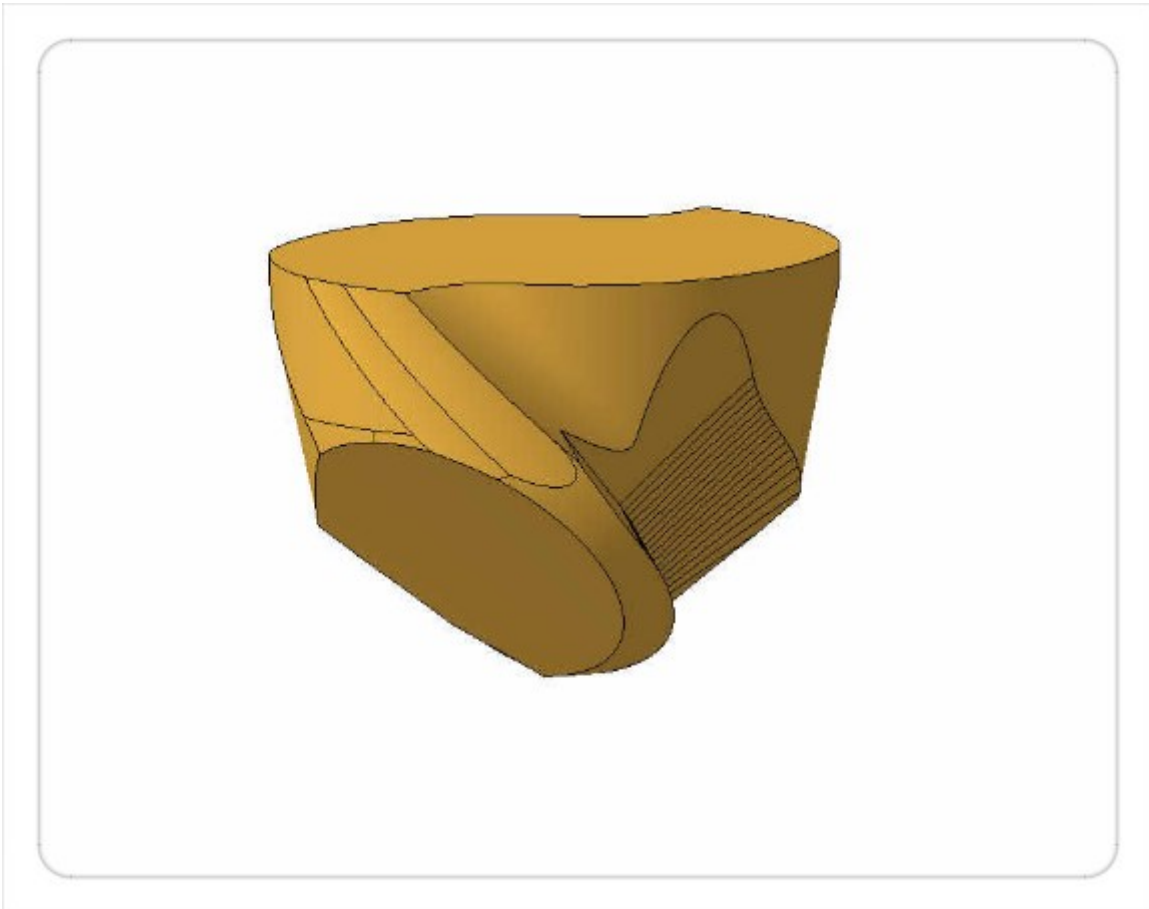
Figure 5.4 Modified Model for Simulation

5.2.2 Machining Parameters

There are several categories of machining operation options in the software, and corner milling matches the conditions to verify the performance of ball end mill. Moreover, both up and down milling is applied for simulation. The dimension of workpiece is 6mm*6mm*4mm. Adaptive remeshing technique is applied in meshing procedure. The section that is approached the more the elements, the more detailed element gets. The minimum element size is 0.15 mm.
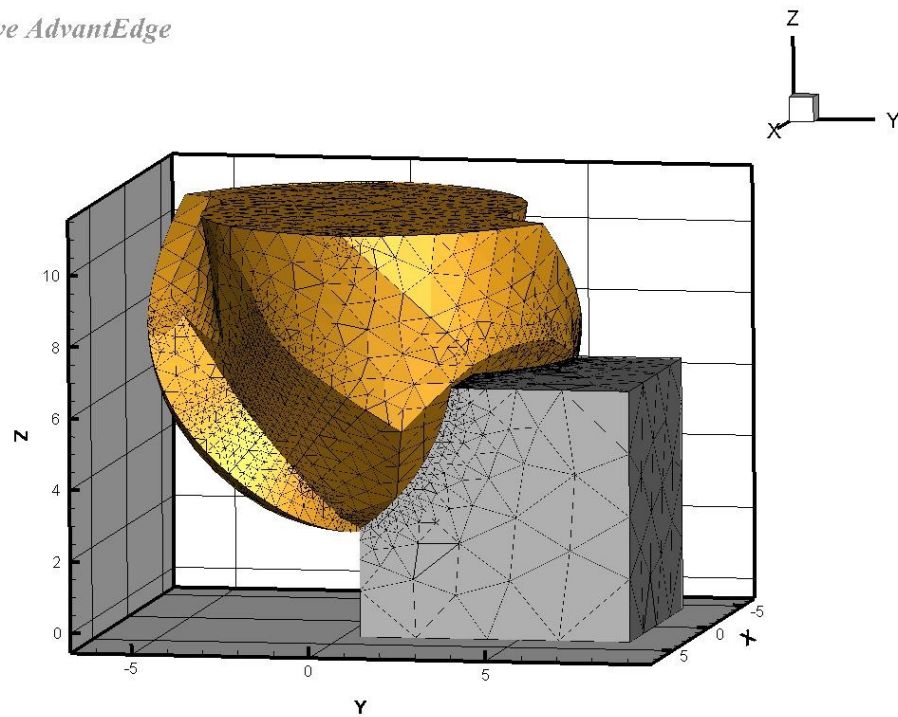
Figure 5.5 Meshing of the Ball End Mill and Workpiece

The meshing of ball end mill is shown in 5.5. Minimum tool element size is 0.1 mm. Runout is not applied in the simulating process, that is because only cutting force

and temperature are tested within 180 degrees that runout of cutter can be neglected.

Figure 0.1 Meshing of fillet end-mill model

Spindle speed can be calculated by

$$RPM = \frac{SFM}{\pi \times \dfrac{1}{12} \times D_\varepsilon}$$ Eq.(5-1)

Where RPM is the spindle speed (revolution per minute), SFM is the linear speed of cutter which is recommended according to different material (160 SFM), Dc is the diameter of cutter stock. After transferring to metric system, the spindle speed for simulation is 1500 r/min. And feed per tooth (FPT) of this cutter for machining Titanium alloy is recommended as 0.1mm/tooth. Fig 5.6 and Fig 5.7 shows the orientation of tool feed and direction of tool motion in terms of down-milling and up-milling, respectively.
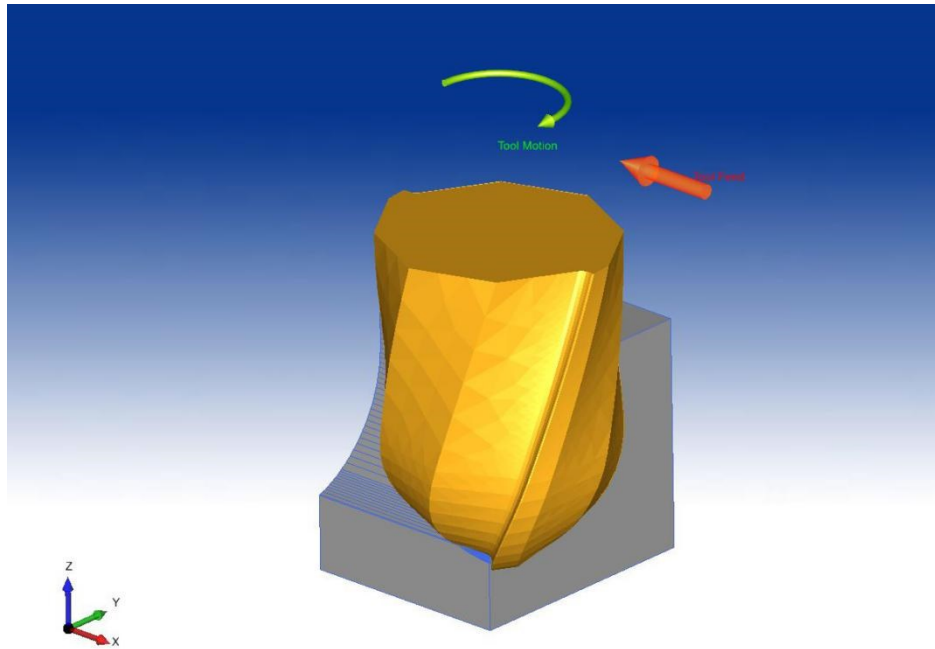
Figure 5.6 Down-milling Tool Feed and Motion
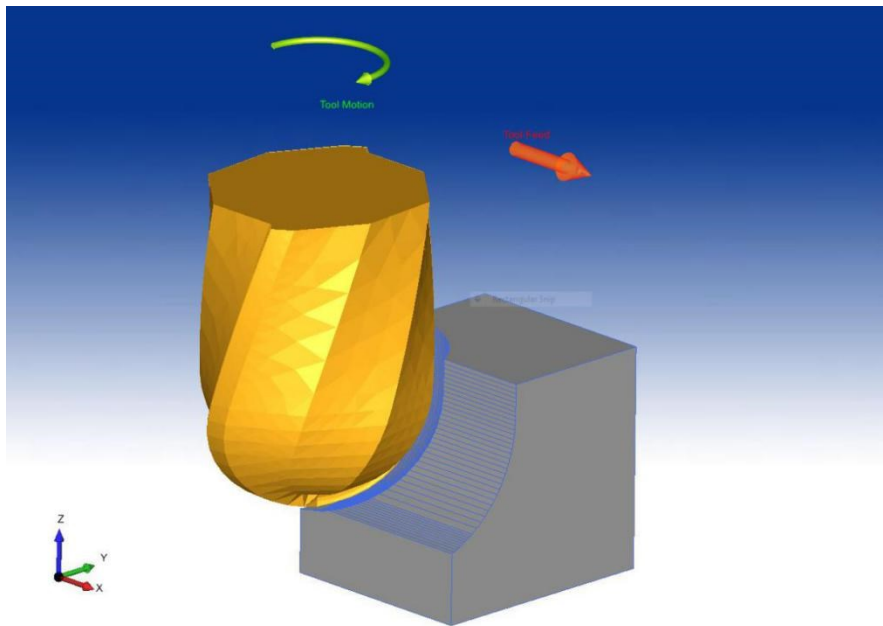
Figure 5.7 Up-milling Tool Feed and Motion

5.3 Simulation Example

After setting the material of tool and workpiece and getting the preparation done, simulating process gets started.

Cutting force is one of the most critical results that reflect the cutting conditions. Besides, by using the cutting force prediction software, we can compare the prediction with the simulation results in order to modify the model avoid stress concentration. Fig 5.8 shows the coordinate system of which the ball end mill is located.
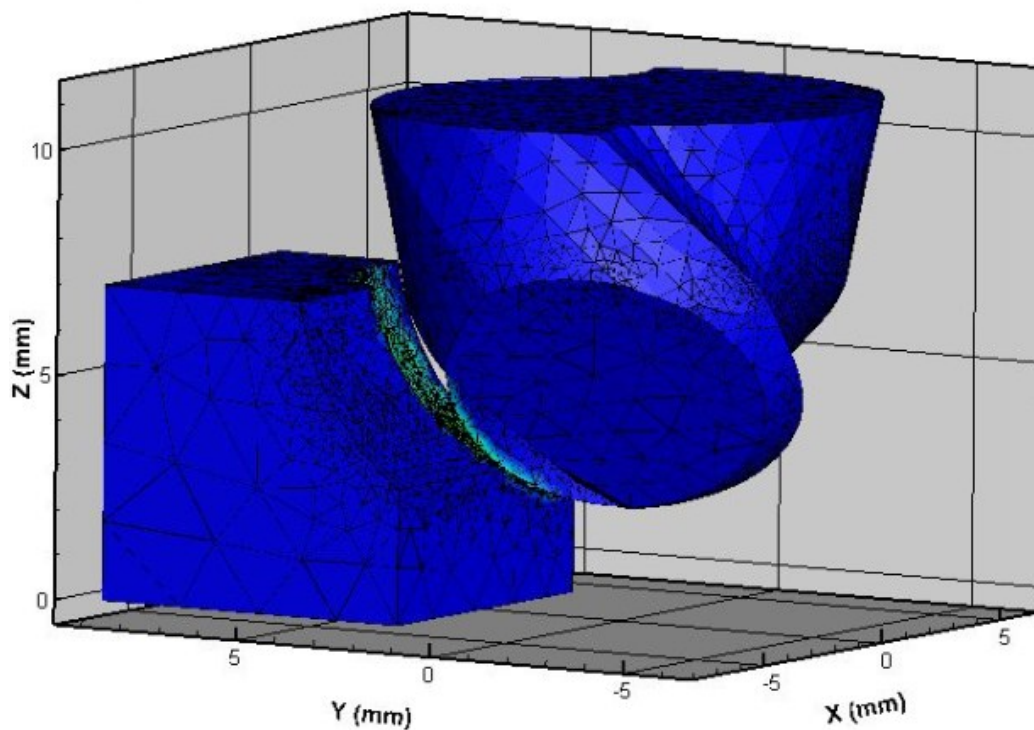
Figure 5.8 Coordinate System of the Tool in AdvantEdge

Cutting forces are derived from simulation on the orientation of X, Y and Z axis. Fig 5.9 indicates that the cutting force variation within 0.0007 seconds. Obviously, in the X-

axis direction, the value of cutting force fluctuate gently. In terms of Y-axis and Z-axis, the value of cutting force changes significantly.
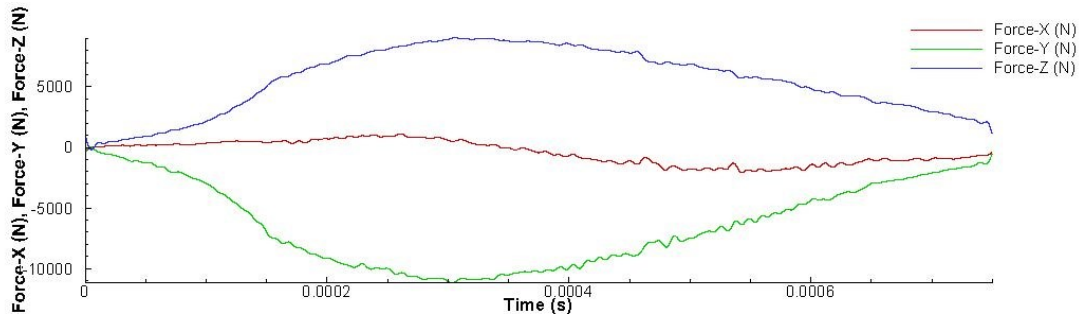
Figure 5.9 Cutting Force Fluctuation Diagram
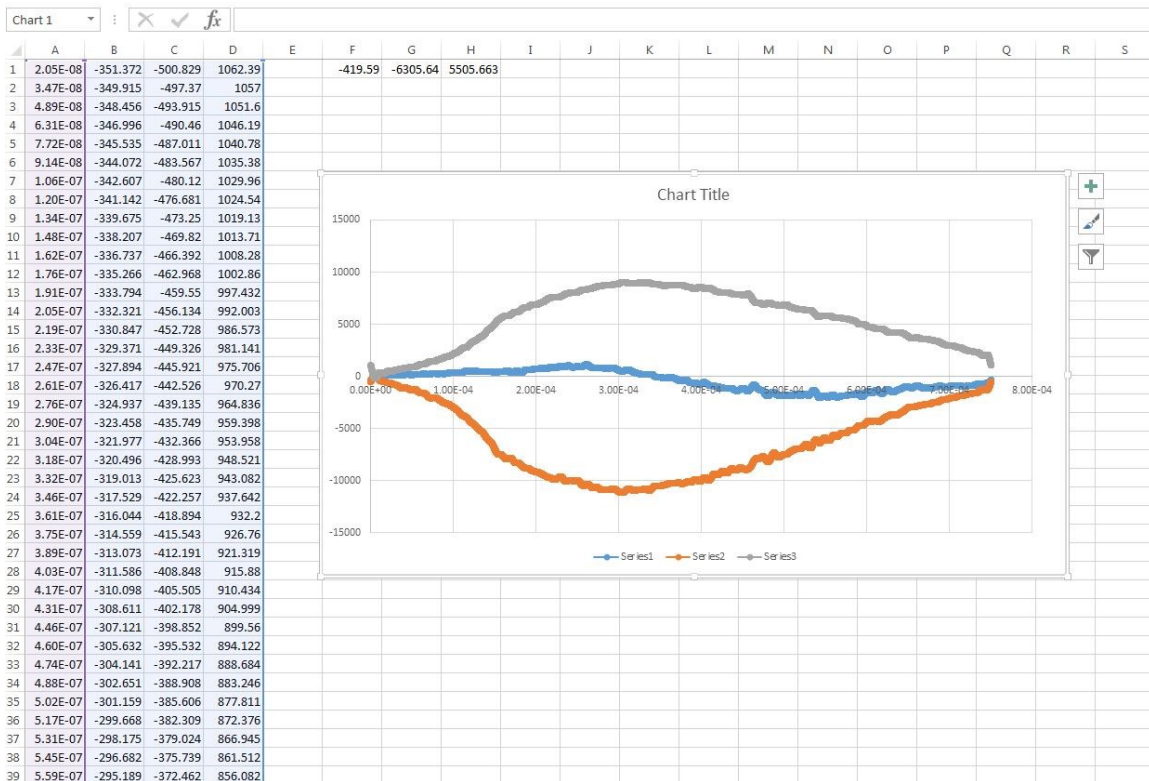
Figure 5.10 Cutting Force Data Analysis in Excel

We can extract the point of the cutting force diagram, and import the data to Microsoft Excel to obtain the average cutting force on each axis orientation.

Thus, the average cutting force of the cutter is obtained. On the direction of X-axis, the cutting force is 419.59 N. On the direction of Y-axis, the cutting force is 6305.64 N. On the direction of Z-axis, the cutting force is 5505.66 N.

Compared with the reviews in the thesis of cutting force prediction [25], the cutting force of this model is too high. Therefore, this will be a consideration of this model in the future work.

Moreover, temperature is an important factor that is effected by the geometry of end mill model. As shown in Fig 5.11, high temperatures are generated in the area of the clearance face. The reason is that the clearance angle we set previously is too small. As a result, there is not enough space for chips evacuation. Hence, the designed clearance angle is required to modify larger.
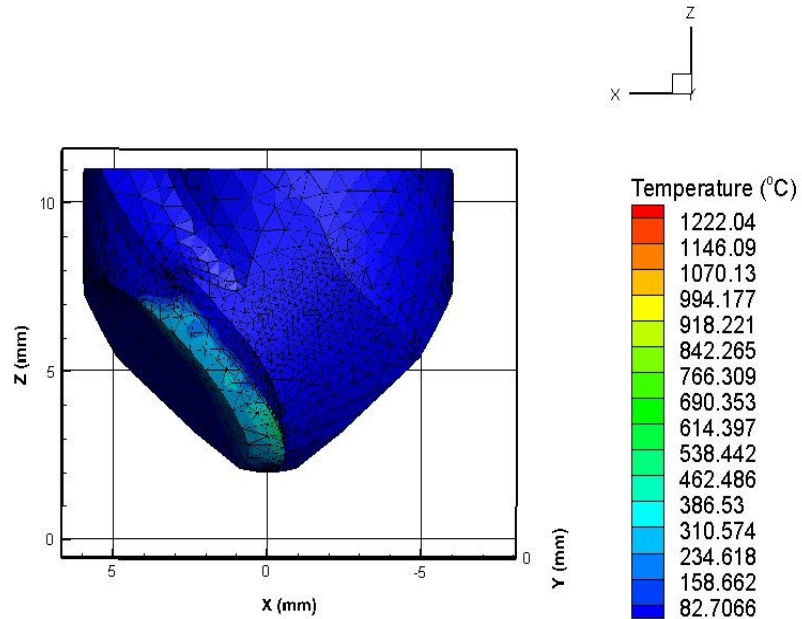
Figure 5.11 Temperature Distribution of the Tool

Chapter 6.Conclusions and Future Work

6.1 Conclusions

In this paper, we build a model of ball end mill, finish the calculation of the basic features of the ball end mill, which are cutting edge curve, bottom curve of rake face, rake face surface. In addition, we integrate the process into a program to obtain the model.

The method of modeling a ball end mill has been introduced, including the determination of the mathematical equations of the basic features of the cutter, the calculation of the grinding wheel location which can lead to NC code generation for the machining process, and the verification of the model via simulation. It follows the principle of current computer aided design, which is combining the mathematical knowledge with computer system to conduct the design covering creation, modification, solid modeling and optimization.

Moreover, in the premise of ensuring the modeling geometric parameters precisely matched with the design parameters, a modeling program is developed to build the model automatically and efficiently. This program saves time significantly so that the new model can be applied to simulation and experiment quickly. It is a way to increase the productivity.

In the simulation part, some problems have been found. The cutting force of designed model is too high, and the clearance angle needs to be modified in order to reduce the temperature on the clearance face.

6.2 Future Work

For the future research, there are several points requires to be considered.

In this research, the designed model is in a two flutes shape. Actually, the amount of the flutes can be modified in the rake face and clearance face modeling program. The multiple flutes ball end mill grinding wheel location will be calculated.

For this model, because the grinding wheel location calculation has been finished, we are able to obtain the NC code by the data of wheel center coordinates and wheel axis orientation vectors. So that further research in machining area will be done in the future.

In the part of simulation, the simulating process will be further discussed by putting into more kinds of material, including more kinds of material match of tools and workpiece. Moreover, the model will be applied into the simulation of freestyle surface machining in the future.

REFERENCES

1. Kim, J. H., Park, J. W., & Ko, T. J. (2008). End mill design and machining via cutting simulation. Computer-Aided Design, 40(3), 324-333.

2. Tandon, P., & Khan, M. R. (2009). Three dimensional modeling and finite element simulation of a generic end mill. Computer-Aided Design, 41(2), 106-114.

3. Lazoglu, I. (2003). Sculpture surface machining: a generalized model of ball-end milling force system. International Journal of Machine Tools and Manufacture, 43(5), 453-462.

4. Altintas, Y., & Lee, P. (1998). Mechanics and dynamics of ball end milling.Journal of Manufacturing Science and Engineering,120(4), 684-692.

5. Vickers, G. W., & Quan, K. W. (1989). Ball-mills versus end-mills for curved surface machining. Journal of Engineering for Industry, 111(1), 22-26.

6. Zhu, R., Kapoor, S. G., & DeVor, R. E. (2001). Mechanistic modeling of the ball end milling process for multi-axis machining of free-form surfaces.Journal of Manufacturing Science and Engineering, 123(3), 369-379.

7. Imani, B. M., Sadeghi, M. H., & Elbestawi, M. A. (1998). An improved process simulation system for ball-end milling of sculptured surfaces.International Journal of Machine Tools and Manufacture, 38(9), 1089-1107.

8. Yucesan, G., & Altintas, Y. (1996). Prediction of ball end milling forces.Journal of engineering for industry,118(1), 95-103.

9. Miyaguchi, T., Masuda, M., Takeoka, E., & Iwabe, H. (2001). Effect of tool stiffness upon tool wear in high spindle speed milling using small ball end mill. Precision engineering, 25(2), 145-154.

10. Gradišek, J., Kalveram, M., & Weinert, K. (2004). Mechanistic identification of specific force coefficients for a general end mill. International Journal of Machine Tools and Manufacture, 44(4), 401-414.

11. Milfelner, M., Kopac, J., Cus, F., & Zuperl, U. (2005). Genetic equation for the cutting force in ball-end milling. Journal of Materials Processing Technology, 164, 1554-1560.

12. Jin, M., Goto, I., Watanabe, T., Kurosawa, J. I., & Murakawa, M. (2007). Development of CBN ball-nosed end mill with newly designed cutting edge.Journal of materials processing technology, 192, 48-54.

13. Sharman, A., Dewes, R. C., & Aspinwall, D. K. (2001). Tool life when high speed ball nose end milling Inconel 718™. Journal of Materials Processing Technology, 118(1), 29-35.

14. Kangnin, M. W. L. Z. C. (1998). Rigid Cutting Force Model of Ball End Mill [J]. MECHANICAL SCIENCE AND TECHNOLOGY, 3.

15. Jinling, X. (1995). The CNC Grinding of the Ball Nose End Mill. TOOL ENGINEERING, 06.

16. Pa, N. M. N., Sarhan, A. A. D., & Shukor, M. H. A. (2012). Optimizing the cutting parameters for better surface quality in 2.5 D cutting utilizing titanium coated carbide ball end mill. International Journal of Precision Engineering and Manufacturing, 13(12), 2097-2102.

17. Imani, B. M., & Elbestawi, M. A. (2001). Geometric simulation of ball-end milling operations. Journal of manufacturing science and engineering, 123(2), 177-184.

18. Kang, M. C., Kim, K. K., Lee, D. W., Kim, J. S., & Kim, N. K. (2001). Characteristics of inclined planes according to the variations of cutting direction in high-speed ball-end milling. The International Journal of Advanced Manufacturing Technology, 17(5), 323-329.

19. Ko, J. H., & Cho, D. W. (2005). 3D ball-end milling force model using instantaneous cutting force coefficients. Journal of manufacturing science and engineering, 127(1), 1-12.

20. Chen, F., & Bin, H. (2009). A novel CNC grinding method for the rake face of a taper ball-end mill with a CBN spherical grinding wheel. The International Journal of Advanced Manufacturing Technology, 41(9-10), 846-857.

21. Lazoglu, I., & Liang, S. Y. (2000). Modeling of ball-end milling forces with cutter axis inclination. Journal of Manufacturing Science and Engineering, 122(1), 3-11.

22. Aoyama, H., Kishinami, T., & Saito, K. (1986). DEVELOPMENT OF THE ELLIPTIC BALL-END-MILL. Bulletin of the Japan Society of Precision Engineering, 20(4), 291-293.

23. Wang, L. M. (2014). A new CAD/CAM/CAE integration approach to modeling flutes of solid end-mills (Doctoral dissertation, Concordia University).

24. Geoffrey Boothroyd, and Winston A. Knight. "Funfamantals of Machining and Machine Tools." CRC Press, 2006: 154.

25. Yang, M., & Park, H. (1991). The prediction of cutting force in ball-end milling. International Journal of Machine Tools and Manufacture, 31(1), 45-54.